Direct Multi–grid Methods for Linear Systems With Harmonic Aliasing Patterns

Pablo Navarrete Michelini

***Abstract*—Multi–level numerical methods that obtain the exact solution of a linear system are presented. The methods are devised by combining ideas from the full multi–grid algorithm and perfect reconstruction filters. The problem is stated as whether a direct solver is possible in a full multi–grid scheme by avoiding smoothing iterations and using different coarse grids at each step. The coarse grids must form a partition of the fine grid and thus establishes a strong connection with domain decomposition methods. An important analogy is established between the conditions for direct solution in multi–grid solvers and perfect reconstruction in filter banks. Furthermore, simple solutions of these conditions for direct multi–grid solvers are found by using mirror filters. As a result, different configurations of direct multi–grid solvers are obtained and studied.**

***Index Terms*—multigrid, perfect reconstruction filter, domain decomposition, direct solver, aliasing.**

I. Introduction

THIS study focuses on the problem of solving the linear system of equations

$$Au = f \tag{1}$$

over the field of complex numbers. The problem is restricted to the case when the number of equations, n, is the same as the number of unknowns, and the number n is even (in some cases a power of 2). The *system matrix* $A \in \mathbb{C}^{n\times n}$ is sparse and it will be assumed to be invertible, with special attention to ill–conditioned cases. The problem becomes challenging when n scales to large numbers (e.g. thousands of unknowns). This situation arises frequently in scientific and engineering computations, most notably in the solution of PDEs [1], [2] and other areas like simulation of stochastic models [3] and the solution of optimization problems [4].

A vast amount of numerical methods exist to solve this problem efficiently. They vary from *direct* (or *exact*) solvers that compute the exact solution, u, to *iterative* solvers that compute a sequence of approximations that converges to the exact solution, $v_k \to u$. Here, convergence must be defined to minimize some norm of the approximation error, $e_k = u - v_k$. Direct solvers are often based on some type of matrix factorization, being the most popular those based on LU decomposition [5], [6]. Among the iterative solvers, the most common are: stationary iterative methods (e.g. Gauss–Seidel, Jacobi and Richardson iterations), Krylov subspace methods (e.g. conjugate gradients, GMRES and BiCG) and multi–level methods (e.g. multi–grid and domain decomposition) [1], [2].

In this study, multi–level numerical methods working as direct solvers are obtained. In the same category there are other direct multi–level solvers like: total reduction methods [7], [8], partial (cyclic) reduction methods [9] and LU factorization of non–standard forms [10]. Besides their structural differences, each method works under certain limitations. Total reduction and partial (cyclic) reduction methods are specifically designed for Poisson's equation, and LU factorization of non–standard forms works for elliptic problems. In this study, the limitations are not described in terms of categories of PDEs but in terms of two additional properties on the system. These are: A has to be diagonalizable, and ignoring some of the unknowns should produce a specific aliasing pattern.

First, by assuming that the system matrix is diagonalizable, we have the eigendecomposition

$$A = W\Lambda V^H , \tag{2}$$

where the columns of W form the set of right eigenvectors, Λ is a diagonal matrix with the eigenvalues of A, and the columns of V form the set of left eigenvectors. Here, the right and left eigenvectors form a *biorthogonal basis* so that $V^H W = I$. This restriction limits the applications to non–defective problems.

The second restriction is on the effects of *down–sampling* the eigenvectors of the system. This operation drops a number of components when applied to vectors and keeps the remaining components untouched. An example is shown in Fig. 1 where one every two samples of harmonic functions are dropped. By down–sampling the eigenvectors of the system their linear independence is lost, because the dimension of the down–sampled space is less than the number of eigenvectors. This is a general description of the phenomenon of *aliasing*. Here, it will be assumed that there is a subset of $n/2$ components defining a down–sampling operation that makes each down–sampled eigenvector equal (up to sign) to only one of the other down–sampled eigenvectors (see Fig. 1). This specific pattern is called *harmonic aliasing* pattern [11] and is found in harmonic functions, which are eigenvectors of *linear*

Manuscript received October 20, 2009; revised January 27, 2010; accepted May 24, 2010. The associate editor coordinating the review of this manuscript and approving it for publication was Prof. Thierry Blu. This work was presented in part at the 14^{th} Copper Mountain Conference on Multigrid Methods, Copper Mountain, CO, USA, March 2009.

The author is with the Department of Electrical Engineering, Universidad de Chile, Santiago, RM, 8370451 Chile.

This paper has supplementary downloadable material available at http://ieeexplore.ieee.org, provided by the author. It includes a set of Scilab programs for solving the example problems in Section VIII, an additional example in Scilab which is recommended to use when reading the paper, and the PSTricks code to generate all the figures. The material is 484 kB in size.

Digital Object Identifier 10.1109/TSP.2010.2053363

Copyright (c) 2010 IEEE. Personal use is permitted. For any other purposes, permission must be obtained from the IEEE by emailing pubs-permissions@ieee.org.

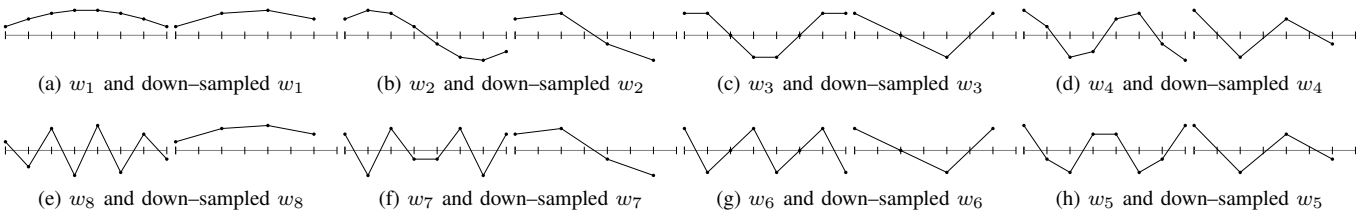

(a) w_1 and down–sampled w_1 (b) w_2 and down–sampled w_2 (c) w_3 and down–sampled w_3 (d) w_4 and down–sampled w_4

(e) w_8 and down–sampled w_8 (f) w_7 and down–sampled w_7 (g) w_6 and down–sampled w_6 (h) w_5 and down–sampled w_5

Fig. 1. Example of harmonic aliasing pattern in a harmonic sine basis. The set of vectors $w_j \in \mathbb{R}^8$, $j = 1, \ldots, 8$, with components $(w_j)_i = \sqrt{\frac{2}{9}}\ \sin(\frac{ij\pi}{9})$, $i = 1, \ldots, 8$ forms an orthonormal basis of $\mathbb{R}^8$. A down–sampling operation drops the components with even i. The resulting down–sampled eigenvectors are not linearly independent. The down–sampling of w_k is equal to the down–sampling of w_{9-k} with $k = 1, \ldots, 4$.

space invariant (LSI) systems[1], and other bases including at least: Hadamard matrices and eigenvectors of coupled systems of equations [11], [12].

The generality of a system with harmonic aliasing patterns is not known at its largest extent. They were introduced in [11] in order to extend the strong convergence analysis of multi–grid algorithms based on *local Fourier analysis* (LFA). This analysis was introduced by Achi Brandt in the late 70's and remains as the main rigorous tool for the design of multi–grid methods [13], [14]. LFA is based on Fourier analysis and is thus restricted to LSI systems, which makes it difficult to use it in many applications. The extended convergence analysis in [11] has not overcome this problem drastically. Nevertheless, in this study its algebraic framework will allow not only the analysis of traditional multi–grid methods but also the introduction of new direct solvers with connections to other important numerical methods.

The contributions of this paper are thus both practical and conceptual. From the practical side, multi–grid algorithms have been successfully applied in many practical problems but the theory behind does not reach the same level. The most common implementation is *algebraic multi–grid* (AMG) which obtains a multi–grid configuration based on heuristics [15]. The numerical methods obtained in this paper represent a step forward on what the theory can achieve. This is, under the assumptions just mentioned, a completely algebraic configuration is found that solves the problem exactly with no use of heuristics. The algorithms are computationally efficient and adaptable to the computational resources (single–core or multi–core).

The conceptual contribution of this paper is the introduction of numerical methods in a setting that establishes a direct analogy between multi–rate systems and different multi–level numerical methods. The analysis exploits the structural similarities of the *full multi–grid algorithm* [16] and problems of signal reconstruction in *multi–rate systems* [17]. On one hand, both classical and extended convergence analysis for multi–grid solvers have shown the importance of aliasing phenomena to explain how the algorithm converges [11], [15]. Here, aliasing appears as an additional source of error that has to be controlled by the algorithm. On the other hand, the problem of signal reconstruction in multi–rate systems follows a different approach. A signal is decomposed in different coarse levels and the question is posed as whether the original signal can be reconstructed from these different pieces of information. Here, each coarse level component has aliasing effects and perfect reconstruction is possible because these effects cancel each other. Given the structural similarities between multi–grid methods and multi–rate system, the central question is whether aliasing cancellation can be used in multi–grid to obtain direct solvers, where the analogue of "perfect reconstruction" is "exact solution."

The connection between multi–grid methods and multi–rate systems itself is not a new topic of research. There have been several efforts to configure multi–grid methods based on the theory of wavelets [18]–[22]. These efforts move around a common aim of using a wavelet decomposition in order to derive the restriction and interpolation operators. On the other hand, the aim of this work follows a different approach. While wavelet decompositions use perfect reconstruction filters in the design of restriction and interpolation operators, the multi–level solvers in this work will not use perfect reconstruction filters at any step of their configuration. Perfect reconstruction filters will only motivate the analogy between "perfect reconstruction" and "exact solution" which stands as the main conceptual contribution.

The main goal, under the assumptions just mentioned, is to modify a full multi–grid algorithm and obtain a direct multi–grid solver in direct analogy with the problem of perfect reconstruction filters. In order to establish this analogy the problem of perfect reconstruction needs to be generalized for systems with harmonic aliasing patterns, which allows to configure perfect reconstruction filters that are not necessarily LSI systems. On the other hand, the full multi–grid algorithm also requires modifications. Multiple coarse grids are needed in order to keep all the information from the original problem in coarse levels. A partition of the complete set of unknowns defines several coarse levels and represents a particular type of *domain decomposition* [23].

Similar approaches can be found in the literature. The use of multiple coarse grids in multi–grid has been introduced by Frederickson and McBryan in [24] and Hackbusch in [25], [26]. It is known that aliasing cancellation helps these methods to converge fast [27]. Nevertheless, none of them work as direct solvers and they use smoothing iterations. Total reduction methods are the closest in structure to the direct

[1]In numerical analysis a different terminology is used. The *stencil* of an unknown is defined as a geometric arrangement of the non–zero coefficients in the correspondent row in A, centered at the diagonal element. This is equivalent to the concept of *impulse response* in signal processing and an LSI system is equivalent to a system with constant stencil coefficients.

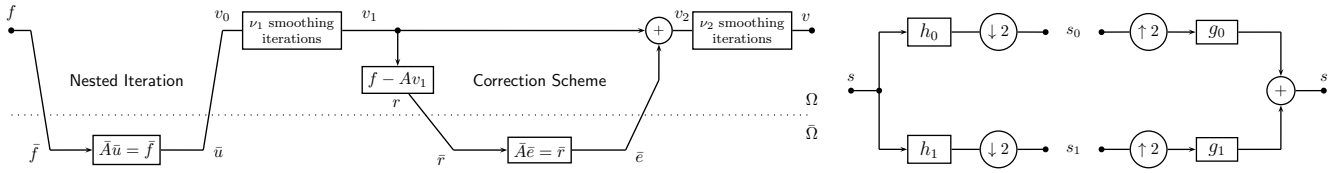

(a) Full two–grid algorithm (b) Two–channel multi–rate system

Fig. 2. The numerical methods introduced in this paper are based on two systems. First, the full two–grid algorithm in Fig. 2a. This is an iterative algorithm to obtain an approximate solution of $Au = f$. The dotted line separates vectors from the fine and coarse grid domains. The interpolation (restriction) operation is applied to vectors crossing the dotted line from below (above). Second, the two–channel multi–rate system in Fig. 2b. Here, each box represents an LSI system and the stationary impulse response is shown inside. The circles with "↓ 2" represent down–sampling operators that drop one every two samples. Similarly, circles with "↑ 2" represent up–sampling operators that insert one zero every two samples.

solvers obtained and can be seen as a more restrictive version of one of the algorithms presented.

In section II, full two–grid algorithms and multi–rate systems are reviewed. In section III, harmonic aliasing patterns are introduced. In section IV, perfect reconstruction filters are studied. In section V, the convergence analysis of two–grid methods is studied. In section VI, the problem of finding direct two–grid solvers is stated and solved. In section VII, the multi–grid case is considered. In section VIII, some examples are presented. And section IX presents some comparisons with other solvers.

II. Preliminaries

A. Full two–grid algorithm

The full two–grid algorithm is an iterative solver used to obtain approximate solutions of (1). In order to simplify the problem, the algorithm uses the concept of *grids* and *coarse grids*. Whatever the nature of the problem is, the system (1) can always be associated with a graph in which the unknowns of the system are the nodes of the graph. The nodes of the graph are associated with a set of labels Ω which is called the *fine grid*. A *coarse grid*, $\bar{\Omega}$, is a proper subset of the fine grid; i.e., $\bar{\Omega} \subset \Omega$.

The so–called *inter–grid operators* are defined as any linear transformation between scalar fields on Ω and $\bar{\Omega}$. That is $\bar{I}_I \in \mathbb{C}^{n\times|\bar{\Omega}|}$ and $\bar{I}_R \in \mathbb{C}^{|\bar{\Omega}|\times n}$, where $\bar{I}_I$ is the *interpolation operator* and $\bar{I}_R$ is the *restriction operator*. In addition to these operations, and following the standard of most multi–grid applications, a coarse system matrix is defined following the *Galerkin condition* [16]

$$\bar{A} \stackrel{\text{def}}{=} \bar{I}_R \, A \, \bar{I}_I \, . \tag{3}$$

A *full two–grid algorithm* solves (1) by using the system shown in Fig. 2a. Here, there are three steps involved. First, two boxes perform fixed numbers of *smoothing* or *stationary iterative* iterations. These iterations –typically Gauss–Seidel, Jacobi, Richardson, etc.– are known to obtain good local approximations of the solution [16]. This means that high–frequency components of the *approximation error*, $e_k = u - v_k$, are efficiently reduced. In each smoothing iteration the approximation error evolves as $e_{k+1} = Se_k$. The matrix S is thus called the *smoothing operator*. For better understanding of this step is convenient to assume that S is a *filter*, or *Fourier multiplier*. If this is the case then S has same eigenvectors as A and it can be decomposed as $S = W\Sigma V^H$. The matrix of eigenvalues, Σ, contains the *frequency response*, or *symbols*, of the smoothing operator. The smoothing effect on the approximation error is seen in the frequency domain as a damping effect concentrated on high–frequency eigenvectors. In other words, the eigen–decomposition of S can be written in block–form as

$$S = W \begin{bmatrix} \Sigma_L & \\ & \Sigma_H \end{bmatrix} V^H \, , \tag{4}$$

where Σ_L and Σ_H correspond to low– and high–frequency eigenvalues close to 1 and 0, respectively.

The remaining steps in Fig. 2a make use of the coarse grid. First, the so–called *nested iteration* step takes f and computes an initial approximation v_0. This step solves a coarse grid equation using a restricted version of the source vector, $\bar{f}$. And second, the so–called *correction scheme* improves the approximation v_1 to obtain v_2. This step computes an approximation of e_k from the error equation $Ae_k = r_k$, where $r_k = f - Av_k$ is the *residual vector* taking the role of the source vector. A coarse grid equation is solved using a restricted version of the source vector, $\bar{r}_k$. Once the approximation is obtained, it is added to correct the current approximation. This step is eventually repeated with smoothing iterations until convergence is achieved.

It is observed that the approximation of e_k obtained in the coarse grid equations effectively represents its low–frequency components and fails to represents its high–frequency components. This is a consequence of the computations in coarse grids where the big picture (low–frequencies) of the solution is clear but details (high–frequencies) are lost.

The approximation error in the coarse grid steps evolves as

$$e_0 = \bar{K}u \quad \text{and} \quad e_{k+1} = \bar{K}e_k \, , \tag{5}$$

for nested iterations and the correction scheme, respectively. Here, the matrix

$$\bar{K} = I - \bar{I}_I \bar{A}^{-1} \bar{I}_R A \tag{6}$$

determines the evolution of the approximation error and is called the *coarse grid correction* matrix [28].

The reduction of low–frequency components of the error in two–grid steps suggests that $\bar{K}$ is a *high–pass filter*. If this would be the case then there would be a decomposition $\bar{K} = W\bar{\Gamma}V^H$ where $\bar{\Gamma}$ is a diagonal matrix. One would expect a frequency response of the filter with the shape shown in Fig.

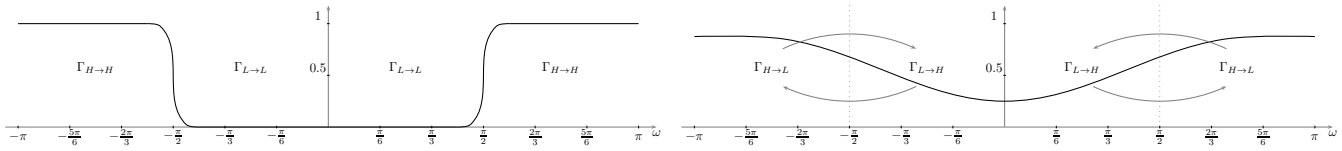

(a) Two–grid filtering effect (b) Two–grid aliasing effect

Fig. 3. Representation of the frequency effects of a coarse grid correction operator in a two–grid algorithm. The operator is not a filter and thus is not completely represented by filtering effects. The operator is completely represented by filtering and aliasing effects. $\bar{\Gamma}_{L\to L}$ indicates the region of low–frequencies where the symbols are close to 0. $\bar{\Gamma}_{H\to H}$ indicates the region of high–frequencies where the symbols are close to 1. $\bar{\Gamma}_{L\to H}$ and $\bar{\Gamma}_{H\to L}$ multiply low– and high–frequencies and take them into high– and low–frequencies, respectively.

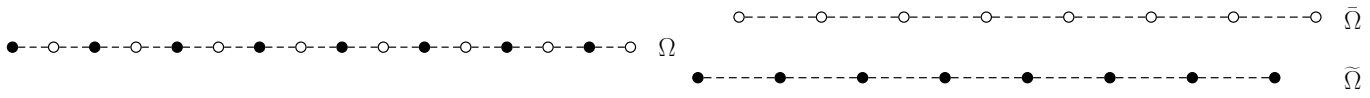

(a) Fine grid with nodes colored red and black. (b) Red and black coarse grids

Fig. 4. Red–black partition of a grid in 1D. The fine grid Ω is partitioned into a red coarse grid $\bar{\Omega}$ and a black coarse grid $\widetilde{\Omega}$.

3a. Unfortunately, this is not the case. $\bar{K}$ is not a filter because of aliasing effects.

Although $\bar{K}$ is not technically a *filter* (or *Fourier multiplier*), under the assumption of harmonic aliasing patterns a decomposition $\bar{K} = W\bar{\Gamma}V^H$ exists where $\bar{\Gamma}$ is sparse (but not diagonal). In the forthcoming sections it will be shown that

$$\bar{K} = W \begin{bmatrix} \bar{\Gamma}_{L\to L} & \bar{\Gamma}_{H\to L} \\ \bar{\Gamma}_{L\to H} & \bar{\Gamma}_{H\to H} \end{bmatrix} V^H , \tag{7}$$

where $\bar{\Gamma}_{L\to L}$, $\bar{\Gamma}_{H\to L}$, $\bar{\Gamma}_{L\to H}$ and $\bar{\Gamma}_{H\to H}$ are all diagonal matrices if one assumes harmonic aliasing patterns. The filtering effect is contained in $\bar{\Gamma}_{L\to L}$ and $\bar{\Gamma}_{H\to H}$, and are expected to be as shown in Fig. 3a. As opposed to a proper filter, this figure does not tell everything about the coarse grid correction matrix. A second graphic, shown in Fig. 3b, must show the aliasing effect from $\bar{\Gamma}_{H\to L}$ and $\bar{\Gamma}_{L\to H}$.

B. Two–channel multi–rate systems

In multi–rate systems one is interested to decompose a discrete signal in different components at lower sampling rates [17], [29]. A two–channel multi–rate system is shown in Fig. 2b. Two restriction operations are performed by filtering and down–sampling. These operations split the original signal, s, into two signals, s_0 and s_1, each with half of the original samples. The original signal is recovered by summing two interpolation operations performed by inserting zeros (up–sampling) and then filtering.

Here, the boxes represent LSI systems which have stationary impulse responses and are filters with respect to a harmonic basis. Their frequency responses are given by the Fourier transforms of their impulse responses: $H_0(\omega)$, $H_1(\omega)$, $G_0(\omega)$ and $G_1(\omega)$. In practical applications the problem is whether the support of the frequency responses can overlap and still be able to recover the original signal. This is possible when the filters fulfill the following conditions by Vetterli [30]

$$G_0(\omega)H_0(\omega) + G_1(\omega)H_1(\omega) = 2 , \tag{8}$$

$$G_0(\omega)H_0(\omega-\pi) + G_1(\omega)H_1(\omega-\pi) = 0 . \tag{9}$$

Here, condition (9) causes the aliasing effects from different channels to cancel each other and (8) causes the final sum to be equal to the original signal. The more general result with an arbitrary number of decompositions is due to Vaidyanathan [31].

III. Red–Black Harmonic Aliasing

A *red* coarse grid, $\bar{\Omega}$, and a *black* coarse grid, $\widetilde{\Omega}$, are defined by a partition of the fine grid. This is, $\Omega = \bar{\Omega} + \widetilde{\Omega}$, where the sum denotes the disjoint union of two sets. An example is shown in Fig. 4. The motivation of the red–black partition is to keep track of all the fine grid nodes in coarser grids. In this way the partition represents a particular type of *domain decomposition* [23].

The selection of nodes to the red and black partition will be represented by *down–sampling* operators according to the following definition.

Definition 1 (Down/Up–sampling matrices): The red and black *down–sampling* matrices are defined as $\bar{D} \in \{0,1\}^{|\bar{\Omega}|\times n}$ and $\widetilde{D} \in \{0,1\}^{|\widetilde{\Omega}|\times n}$ such that

$$(\bar{D})_{i,j} \stackrel{\text{def}}{=} \begin{cases} 1 & \text{if node } j \in \Omega \text{ is the } i^{th} \text{ red node in } \bar{\Omega} \\ 0 & \text{otherwise} \end{cases} \tag{10}$$

and

$$(\widetilde{D})_{i,j} \stackrel{\text{def}}{=} \begin{cases} 1 & \text{if node } j \in \Omega \text{ is the } i^{th} \text{ black node in } \widetilde{\Omega} \\ 0 & \text{otherwise} \end{cases} , \tag{11}$$

respectively. Similarly, the red and black *up–sampling* matrices are defined as $\bar{U} \in \{0,1\}^{n\times|\bar{\Omega}|}$ and $\widetilde{U} \in \{0,1\}^{n\times|\widetilde{\Omega}|}$ such that $\bar{U} = \bar{D}^T$ and $\widetilde{U} = \widetilde{D}^T$, respectively.

The down–sampling matrix of a certain color represents a linear transformation that takes a fine grid vector and drops all the values that correspond to a node of different color. The up–sampling matrix takes a coarse grid vector and inserts zeros at the new nodes (of different color) in the fine grid. From this

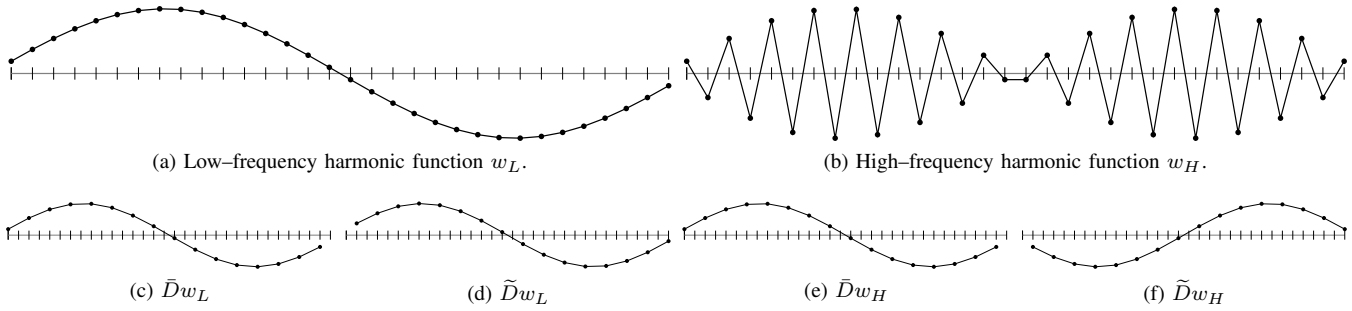

(a) Low–frequency harmonic function w_L. (b) High–frequency harmonic function w_H.

(c) $\bar{D}w_L$ (d) $\widetilde{D}w_L$ (e) $\bar{D}w_H$ (f) $\widetilde{D}w_H$

Fig. 5. Difference between red and black harmonic aliasing patterns. The red down–sampling of w_L and w_H are equal, $\bar{D}w_L = \bar{D}w_H$. Whereas the black down–sampling of w_L is the negative of the black down–sampling of w_H, $\widetilde{D}w_L = -\widetilde{D}w_H$.

interpretation, a set of basic properties follows

$$\bar{D}\bar{U} = I \quad \text{and} \quad \widetilde{D}\widetilde{U} = I \,, \tag{12}$$

$$\widetilde{D}\bar{U} = 0 \quad \text{and} \quad \bar{D}\widetilde{U} = 0 \,, \quad \text{and} \tag{13}$$

$$\bar{U}\bar{D} + \widetilde{U}\widetilde{D} = I \,. \tag{14}$$

In [11] a so–called *harmonic aliasing* pattern was defined only for the red grid. The following definition considers both red and black grids. This addition has important consequences in the results to come.

Definition 2 (Red and Black Harmonic Aliasing Patterns): A matrix $M \in \mathbb{C}^{n\times n}$ is said to have *red* and *black harmonic aliasing patterns* if it is diagonalizable, with biorthogonal eigenvectors W and V, and there exists a red–black partition which divides the domain into two halves, with down–sampling matrices $\bar{D} \in \{0,1\}^{\frac{n}{2}\times n}$ and $\widetilde{D} \in \{0,1\}^{\frac{n}{2}\times n}$, such that

$$V^H\bar{U}\bar{D}W = \bar{N} \quad \text{and} \quad V^H\widetilde{U}\widetilde{D}W = \widetilde{N} \,, \tag{15}$$

respectively. Here, $\bar{N}$ and $\widetilde{N}$ are the *red* and *black harmonic aliasing patterns* defined, respectively, as

$$\bar{N} \stackrel{\text{def}}{=} \frac{1}{2}\begin{bmatrix} I & I \\ I & I \end{bmatrix} \quad \text{and} \quad \widetilde{N} \stackrel{\text{def}}{=} \frac{1}{2}\begin{bmatrix} I & -I \\ -I & I \end{bmatrix} \,. \tag{16}$$

In this definition the red and black harmonic aliasing patterns appear as independent properties. The following statement shows how these definitions are equivalent.

Proposition 1: A matrix with red harmonic aliasing pattern has black harmonic aliasing pattern, and vice versa. Therefore, a matrix with these properties is said to have a red–black harmonic aliasing pattern.

Proof: Taking (14), pre–multiplied by V^H and post–multiplied by W gives

$$V^H\bar{U}\bar{D}W + V^H\widetilde{U}\widetilde{D}W = I \,. \tag{17}$$

Thus, if $V^H\bar{U}\bar{D}W = \bar{N}$ then $V^H\widetilde{U}\widetilde{D}W = \widetilde{N}$, and vice versa. ∎

The definition of red–black harmonic aliasing pattern is convenient for algebraic manipulation but the connection with the common concept of aliasing is not clear yet. In the following theorem an alternative and equivalent definition is given which makes this connection explicit.

Theorem 1 (Navarrete and Coyle): A matrix $M \in \mathbb{C}^{n\times n}$ with red–black harmonic aliasing pattern is equivalent to have a diagonalizable matrix, with biorthogonal eigenvectors W and V, for which there exists a red–black partition dividing the domain into two halves, with down–sampling matrices $\bar{D} \in \{0,1\}^{\frac{n}{2}\times n}$ and $\widetilde{D} \in \{0,1\}^{\frac{n}{2}\times n}$, and such that there is an ordering of the eigenvectors for which the partitions $W = [W_L W_H]$ and $V = [V_L V_H]$ fulfill the conditions

$$\bar{D}W_L = \bar{D}W_H \,, \qquad \bar{D}V_L = \bar{D}V_H \,, \tag{18}$$

$$\widetilde{D}W_L = -\widetilde{D}W_H \quad \text{and} \qquad \widetilde{D}V_L = -\widetilde{D}V_H. \tag{19}$$

The proof of this theorem is partially contained in [11] were only the red coarse grid was considered. The result for the black coarse grid is shown in Appendix A.

The sign difference between the red and black harmonic aliasing patterns is explained in Fig. 5 and it represents the fact that harmonic basis vectors are composed of two envelopes which, intermixed with the same sign form a low frequency and, intermixed with opposed signs form a high–frequency.

The definition of red–black harmonic aliasing patterns for a given matrix does not involve its eigenvalues. But, in the algebra derived from the partition of eigenvectors in Theorem 1 it will be necessary to specify which eigenvalues are associated to each partition. The following remark introduces the notation to make this distinction clear.

Remark 1: For a matrix $M \in \mathbb{C}^{n\times n}$ with red–black harmonic aliasing patterns and eigen–decomposition $M = WEV^H$, the partition of eigenvectors, $W = [W_L W_H]$ and $V = [V_L V_H]$, induces a partition of eigenvalues such that $E = \left[\begin{smallmatrix} E_L & \\ & E_H \end{smallmatrix}\right]$, where E_L and E_H are the diagonal matrices of eigenvalues associated with L and H eigenvectors, respectively.

IV. Perfect Reconstruction Filters for Systems with Harmonic Aliasing Patterns

In the context of finite discrete systems we want to extend the idea of perfect reconstruction filters for systems with harmonic aliasing patterns, which are more general than LSI systems. First, we define an object that will extend the operation of quadrature mirror filters [32]–[34].

Definition 3 (Mirror Matrix): The *mirror* of a matrix $M \in \mathbb{C}^{n\times n}$ with respect to a red–black partition represented by down/up–sampling matrices $\bar{D}$, $\bar{U} = \bar{D}^T$, and $\widetilde{D}$, $\widetilde{U} = \widetilde{D}^T$, is defined as

$$M^\star \stackrel{\text{def}}{=} (\bar{U}\bar{D} - \widetilde{U}\widetilde{D})M(\bar{U}\bar{D} - \widetilde{U}\widetilde{D}) \,. \tag{20}$$

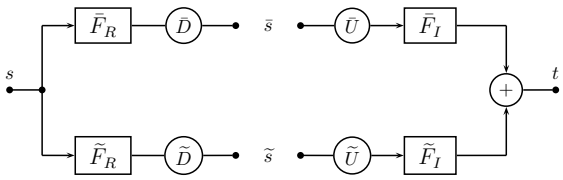

Fig. 6. Two–channel finite multi–rate system. The system takes a signal $s \in \mathbb{C}^n$, decomposes it into $\bar{s} \in \mathbb{C}^{n/2}$ and $\tilde{s} \in \mathbb{C}^{n/2}$, and recovers $t \in \mathbb{C}^n$. A perfect reconstruction system is such that $t = s$. Here, $\bar{F}_R$ and $\widetilde{F}_R$ are restriction filters; $\bar{F}_I$ and $\widetilde{F}_I$ are interpolation filters; $\bar{D}$ and $\widetilde{D}$ represent down–sampling operations; and, $\bar{U}$ and $\widetilde{U}$ represent up–sampling operations.

Matrices $\bar{U}\bar{D} \in \{0,1\}^{n\times n}$ and $\widetilde{U}\widetilde{D} \in \{0,1\}^{n\times n}$ are diagonal with one's whenever $i = j$ is a red or black node, respectively, and zero otherwise. Therefore, $\bar{U}\bar{D} - \widetilde{U}\widetilde{D}$ is a diagonal matrix that takes the value 1 when $i = j$ is a red node, and takes the value -1 when $i = j$ is a black node.

For an LSI system with stationary impulse response $h[n]$, the mirror operator with respect to a uniform down–sampling by factor of 2 (where red nodes are even nodes) produces an impulse response $h^\star[n] = (-1)^n h[n]$. This filter has symbols $H^\star(\omega) = H(\omega - \pi)$ and thus swaps low and high frequencies. The following proposition generalizes this result to systems with red–black harmonic aliasing patterns.

Proposition 2: The mirror of a matrix $M \in \mathbb{C}^{n\times n}$ with red–black harmonic aliasing patterns and eigen–decomposition $M = W \left[\begin{smallmatrix} E_L & \\ & E_H \end{smallmatrix}\right] V^H$, is a filter with eigen–decomposition

$$M^\star = W \begin{bmatrix} E_H & \\ & E_L \end{bmatrix} V^H \,. \tag{21}$$

Proof: Using the eigen–decomposition of M and the definition of red and black harmonic aliasing patterns, the result is obtained as follows

$$\begin{aligned} M^\star &= WV^H(\bar{U}\bar{D} - \widetilde{U}\widetilde{D})W\; E\; V^H(\bar{U}\bar{D} - \widetilde{U}\widetilde{D})WV^H \\ &= W \left[\begin{smallmatrix} 0 & I \\ I & 0 \end{smallmatrix}\right] \left[\begin{smallmatrix} E_L & 0 \\ 0 & E_H \end{smallmatrix}\right] \left[\begin{smallmatrix} 0 & I \\ I & 0 \end{smallmatrix}\right] V^H \\ &= W \left[\begin{smallmatrix} E_H & \\ & E_L \end{smallmatrix}\right] V^H \,. \end{aligned} \tag{22}$$

■

These results are all we need to proceed into the results of the next sections. Now, in order to show the analogy between perfect reconstruction filters and direct multi–grid solvers we have to look back to the problem of perfect reconstruction and see how the main results look for systems with harmonic aliasing patterns. First, we need to restrict the problem to discrete signals in $\mathbb{C}^n$. The two–channel multi–rate system in Fig. 6 is then the finite and discrete version of the system in Fig. 2b. The problem is to find interpolation and restriction matrices $\bar{F}_I$, $\bar{F}_R$, $\widetilde{F}_I$ and $\widetilde{F}_R$ in $\mathbb{C}^{n\times n}$ that are filters with respect to a biorthogonal basis W and V, and such that we have perfect reconstruction; i.e., $t = s$.

The following theorem restates Vetterli's conditions (8) and (9) in this new context.

Theorem 2 (Vetterli): Let $\bar{F}_I$, $\bar{F}_R$, $\widetilde{F}_I$ and $\widetilde{F}_R$ be filters with respect to a biorthogonal basis W and V in $\mathbb{C}^{n\times n}$. Let their matrices of eigenvalues be $\bar{\Pi}_I$, $\bar{\Pi}_R$, $\widetilde{\Pi}_I$ and $\widetilde{\Pi}_R$, respectively, and the eigenvectors have red–black harmonic aliasing patterns with respect to the down–sampling matrices $\bar{D}$ and $\widetilde{D}$. Then, the multi–rate system in Fig. 6 has the perfect reconstruction property, $t = s$, if and only if

$$\bar{\Pi}_I\bar{\Pi}_R + \widetilde{\Pi}_I\widetilde{\Pi}_R = 2I \,, \tag{23}$$

$$\bar{\Pi}_{I,L}\bar{\Pi}_{R,H} - \widetilde{\Pi}_{I,L}\widetilde{\Pi}_{R,H} = 0 \,, \text{ and} \tag{24}$$

$$\bar{\Pi}_{I,H}\bar{\Pi}_{R,L} - \widetilde{\Pi}_{I,H}\widetilde{\Pi}_{R,L} = 0 \,, \tag{25}$$

where the L and H subindexes follow the notation introduced in Remark 1.

Proof: From Fig. 6, perfect reconstruction is obtained if and only if

$$\bar{F}_I\bar{U}\bar{D}\bar{F}_R + \widetilde{F}_I\widetilde{U}\widetilde{D}\widetilde{F}_R = I \,. \tag{26}$$

Pre–multiplying by V^H, post–multiplying by W and using the definitions in (15) gives

$$\tfrac{1}{2}\begin{bmatrix} \bar{\Pi}_{I,L}\bar{\Pi}_{R,L}+\widetilde{\Pi}_{I,L}\widetilde{\Pi}_{R,L} & \bar{\Pi}_{I,L}\bar{\Pi}_{R,H}-\widetilde{\Pi}_{I,L}\widetilde{\Pi}_{R,H} \\ \bar{\Pi}_{I,H}\bar{\Pi}_{R,L}-\widetilde{\Pi}_{I,H}\widetilde{\Pi}_{R,L} & \bar{\Pi}_{I,H}\bar{\Pi}_{R,H}+\widetilde{\Pi}_{I,H}\widetilde{\Pi}_{R,H} \end{bmatrix} = \left[\begin{smallmatrix} I & 0 \\ 0 & I \end{smallmatrix}\right] \,. \tag{27}$$

The blocks in the diagonal are equivalent to (23) and the off–diagonals give (24) and (25). ■

Next, we are interested in a particular solution of these conditions using mirror filters. The following corollary generalizes the solution using *quadrature mirror* filters (QMF) for perfect reconstruction in a two–channel multi–rate system with respect to a biorthogonal basis with red–black harmonic aliasing patterns.

Corollary 1 (Croisier et al.): Perfect reconstruction conditions (23), (24) and (25) are fulfilled if $\bar{F}_I$ is such that

$$\bar{\Pi}_{I,L}^2 + \bar{\Pi}_{I,H}^2 = 2I \,, \quad \text{and} \tag{28}$$

$$\bar{F}_R = \bar{F}_I \,, \quad \widetilde{F}_I = \bar{F}_I^\star \,, \text{ and } \quad \widetilde{F}_R = \bar{F}_I^\star \,. \tag{29}$$

Proof: Using Proposition 2, if (29) is assumed then the conditions (24) and (25) are fulfilled. The mirror condition (28) is necessary to fulfill (23). ■

Quadrature mirror filters were introduced as a solution of the perfect reconstruction problem in [32]. In its original formulation, only a Haar filter gives a sparse quadrature mirror filter [35]. Later, this problem was solved by the introduction of conjugate mirror filters [33], [34], and later generalized for biorthogonal and multi–channel paraunitary systems [30], [31]. The problem to obtain perfect reconstruction FIR filters has to do with the delays between the filters. From a signal processing perspective the red–black partition corresponds to a *polyphase decomposition* [17], [29], [36] that introduces the delays in the down/up–sampling operations and allows to obtain the different solutions for perfect reconstruction.

V. Two–Grid Convergence

Since the configuration of a two–grid algorithm involves many parameters and assumptions, it is convenient to introduce a single terminology that refers to this configuration.

Definition 4 (Red–Black Harmonic Two–grid Configuration): A *red–black harmonic two–grid configuration* is a set of matrices depending on a system matrix $A \in \mathbb{C}^{n\times n}$ with red–black harmonic aliasing patterns and biorthogonal eigenvectors W and V. The red–black partition of nodes is represented by down–sampling operators $\bar{D}$ and $\widetilde{D}$. The

configuration is completed with the inter–grid filters $\bar{F}_R$, $\bar{F}_I$, $\widetilde{F}_R$ and $\widetilde{F}_I$, all in $\mathbb{C}^{n\times n}$. Then, a series of matrices associated with the configuration are defined. First, the interpolation and restriction operators, and the two coarse system matrices given by the Galerkin condition, are defined as

$$\bar{I}_R = \bar{D}\bar{F}_R\,, \quad \bar{I}_I = \bar{F}_I\bar{U}\,, \quad \widetilde{I}_R = \widetilde{D}\widetilde{F}_R\,, \ \widetilde{I}_I = \widetilde{F}_I\widetilde{U}\,, \tag{30}$$

$$\bar{A} = \bar{I}_R A \bar{I}_I \quad \text{and} \quad \widetilde{A} = \widetilde{I}_R A \widetilde{I}_I\,. \tag{31}$$

The system matrix and the inter–grid filters have eigen–decompositions

$$\begin{aligned} A &= W\,\Lambda\,V^H\,,\\ \bar{F}_R &= W\,\bar{\Pi}_R\,V^H\,, \qquad \bar{F}_I = W\,\bar{\Pi}_I\,V^H\,,\\ \widetilde{F}_R &= W\,\widetilde{\Pi}_R\,V^H \quad \text{and} \quad \widetilde{F}_I = W\,\widetilde{\Pi}_I\,V^H\,, \end{aligned}$$

and the partition of eigenvectors, $W = [W_L W_H]$ and $V = [V_L V_H]$, leads to the partitions of eigenvalues

$$\begin{aligned} \Lambda &= \begin{bmatrix} \Lambda_L & \\ & \Lambda_H \end{bmatrix},\\ \bar{\Pi}_R &= \begin{bmatrix} \bar{\Pi}_{R,L} & \\ & \bar{\Pi}_{R,H} \end{bmatrix}, \qquad \bar{\Pi}_I = \begin{bmatrix} \bar{\Pi}_{I,L} & \\ & \bar{\Pi}_{I,H} \end{bmatrix},\\ \widetilde{\Pi}_R &= \begin{bmatrix} \widetilde{\Pi}_{R,L} & \\ & \widetilde{\Pi}_{R,H} \end{bmatrix} \quad \text{and} \quad \widetilde{\Pi}_I = \begin{bmatrix} \widetilde{\Pi}_{I,L} & \\ & \widetilde{\Pi}_{I,H} \end{bmatrix}. \end{aligned}$$

Finally, the two coarse grid correction matrices are defined as

$$\bar{K} = I - \bar{I}_I\bar{A}^{-1}\bar{I}_R A \quad \text{and} \tag{32}$$

$$\widetilde{K} = I - \widetilde{I}_I\widetilde{A}^{-1}\widetilde{I}_R A\,. \tag{33}$$

Now, based on these definitions, the goal is to obtain an eigen–decomposition of the coarse grid correction matrices. The following lemma takes the first step by giving useful expressions for the inverse of the coarse system matrices in (32) and (33).

Lemma 1 (Navarrete and Coyle): In a red–black harmonic two–grid configuration the inverses of the red and black coarse grid matrices are given by

$$\bar{A}^{-1} = 4\,(\bar{D}W_L)\bar{\Delta}^{-1}(\bar{D}V_L)^H \quad \text{and} \tag{34}$$

$$\widetilde{A}^{-1} = 4\,(\widetilde{D}W_L)\widetilde{\Delta}^{-1}(\widetilde{D}V_L)^H\,, \tag{35}$$

respectively, with

$$\bar{\Delta} = \bar{\Pi}_{R,L}\Lambda_L\bar{\Pi}_{I,L} + \bar{\Pi}_{R,H}\Lambda_H\bar{\Pi}_{I,H} \quad \text{and} \tag{36}$$

$$\widetilde{\Delta} = \widetilde{\Pi}_{R,L}\Lambda_L\widetilde{\Pi}_{I,L} + \widetilde{\Pi}_{R,H}\Lambda_H\widetilde{\Pi}_{I,H}\,. \tag{37}$$

The proof of this lemma is partially contained in [11] were only the red coarse grid was considered. The proof for the black grid is shown in Appendix B.

The result in Lemma 1 reflects the structure of a system with harmonic aliasing patterns. The eigenvectors of coarse system matrices are given by a linear–independent subset of the down–sampling eigenvectors of the system matrix. The coarse eigenvalues are expressed as sums of low– and high–frequency eigenvalues as a result of aliasing effects.

Finally, the following theorem gives the eigen–decompositions of coarse grid correction matrices.

Theorem 3 (Navarrete and Coyle): In a red–black harmonic two–grid configuration the red and black coarse grid correction matrices (32) and (33) can be decomposed as

$$\bar{K} = W \begin{bmatrix} \bar{\Gamma}_{L\to L} & \bar{\Gamma}_{H\to L} \\ \bar{\Gamma}_{L\to H} & \bar{\Gamma}_{H\to H} \end{bmatrix} V^H \quad \text{and} \tag{38}$$

$$\widetilde{K} = W \begin{bmatrix} \widetilde{\Gamma}_{L\to L} & \widetilde{\Gamma}_{H\to L} \\ \widetilde{\Gamma}_{L\to H} & \widetilde{\Gamma}_{H\to H} \end{bmatrix} V^H\,, \tag{39}$$

with

$$\begin{aligned} \bar{\Gamma}_{L\to L} &= I - \bar{\Pi}_{I,L}\bar{\Delta}^{-1}\bar{\Pi}_{R,L}\Lambda_L\,,\\ \bar{\Gamma}_{H\to L} &= -\bar{\Pi}_{I,L}\bar{\Delta}^{-1}\bar{\Pi}_{R,H}\Lambda_H\,,\\ \bar{\Gamma}_{L\to H} &= -\bar{\Pi}_{I,H}\bar{\Delta}^{-1}\bar{\Pi}_{R,L}\Lambda_L\,,\\ \bar{\Gamma}_{H\to H} &= I - \bar{\Pi}_{I,H}\bar{\Delta}^{-1}\bar{\Pi}_{R,H}\Lambda_H \end{aligned}$$

and

$$\begin{aligned} \widetilde{\Gamma}_{L\to L} &= I - \widetilde{\Pi}_{I,L}\widetilde{\Delta}^{-1}\widetilde{\Pi}_{R,L}\Lambda_L\,,\\ \widetilde{\Gamma}_{H\to L} &= \widetilde{\Pi}_{I,L}\widetilde{\Delta}^{-1}\widetilde{\Pi}_{R,H}\Lambda_H\,,\\ \widetilde{\Gamma}_{L\to H} &= \widetilde{\Pi}_{I,H}\widetilde{\Delta}^{-1}\widetilde{\Pi}_{R,L}\Lambda_L\,,\\ \widetilde{\Gamma}_{H\to H} &= I - \widetilde{\Pi}_{I,H}\widetilde{\Delta}^{-1}\widetilde{\Pi}_{R,H}\Lambda_H\,. \end{aligned}$$

The proof of this theorem is partially contained in [11] were only the red coarse grid was considered. The result for the black coarse grid is shown in Appendix C.

The results for the red and black coarse grids carry the difference in sign from the definition of harmonic aliasing patterns, which can be seen in the cross–modal symbols ($H \to L$ and $L \to H$).

VI. Direct Two–Grid Methods

In this section the full two–grid algorithm shown in Fig. 2a will be modified to obtain direct two–grid solvers for systems with harmonic aliasing patterns. The motivation is to eliminate smoothing iterations in the full two–grid scheme and base the algorithm purely on nested iterations and/or correction schemes.

A mere elimination of smoothing iterations in Fig. 2a would make it impossible for the algorithm to converge since partial information in a single coarse grid is not enough to get all the information from the fine grid. The algebra is very clear on this point because, based on the Galerkin condition, a coarse grid correction matrix is idempotent (or projection matrix). This is,

$$\bar{K}^2 = \bar{K} \quad \text{and} \quad \widetilde{K}^2 = \widetilde{K}\,, \tag{40}$$

which means that several iterations of two–grid steps with a single coarse grid do nothing more than a single iteration. On the other hand, the red–black partition keeps all the information from the fine grid. Therefore, combining red and black coarse grids at different steps of the algorithm has a chance to converge depending on the configuration of the algorithm.

A. Multiplicative Approach

Two modifications of the full two–grid algorithm from Fig. 2a are considered in Fig. 7a. First, smoothing iterations are removed. And second, red and black coarse grids are considered in the nested iteration and correction scheme steps, respectively.

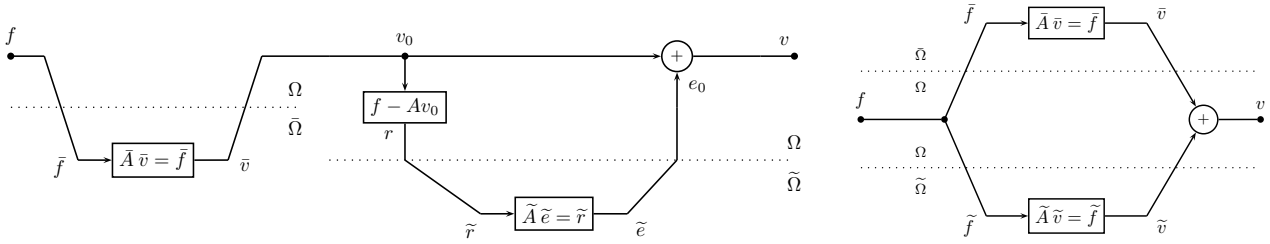

(a) Multiplicative scheme (b) Additive scheme

Fig. 7. Two–grid schemes approaches to solve $Au = f$ exactly. The multiplicative scheme is different than the full two–grid scheme shown in Fig. 2a because no smoothing iterations are used, and different coarse grids are used at each step. The additive scheme is the two–grid algorithm's version of the two–channel multi–rate system in Fig. 6. In both cases the two coarse grids form a partition of the fine grid and thus capture all the information from the fine grid. This fact allows these schemes to work as direct solvers; i.e., allows $v = u$.

If this algorithm works as a direct solver then it means that the problem is being factorized into coarse grid sub–problems. The following proposition shows this in terms of a factorization of A^{-1}.

Proposition 3: The system shown in Fig. 7a works as a direct solver; i.e., $v = u$, if and only if the following decomposition applies on the inverse of the system matrix:

$$A^{-1} = \bar{I}_I \bar{A}^{-1} \bar{I}_R + \widetilde{I}_I \widetilde{A}^{-1} \widetilde{I}_R - \widetilde{I}_I \widetilde{A}^{-1} (\widetilde{I}_R A \bar{I}_I) \bar{A}^{-1} \bar{I}_R \ . \quad (41)$$

Proof: Using (5) in Fig. 7a gives

$$e = \widetilde{K} \bar{K} u \ . \quad (42)$$

Then, an exact solution is obtained if and only if $\widetilde{K}\bar{K} = 0$. Using (32) and (33) gives (41). ∎

In this matrix factorization, the first two terms indicate the components of the inverse that come from the red and coarse grids independently. The third term indicates the dependence between the two solutions. In fact, the correction scheme in Fig. 7a works on top of the solution given by nested iteration and thus mixes the solutions from both coarse grids.

This factorization is known in domain decompositions as the *multiplicative Schwartz procedure* [23]. In this procedure the evolution of the approximation error in m iteartions is represented by the *multiplicative operator*, $P_{mu} = I - E_{mu}$. Here, $E_{mu} = K_m \cdots K_1 K_0$ and K_i are coarse grid correction matrices. The classical domain decomposition approach does not work as a direct solver and therefore $P_{mu} \neq I$. Thus, the two–grid configuration in Fig. 7a corresponds to a direct multiplicative Schwartz configuration.

The following theorem establishes conditions on the inter–grid filters to obtain a direct solver.

Theorem 4: A red–black harmonic two–grid configuration arranged as shown in Fig. 7a, with non–singular A, $\bar{A}$, $\bar{F}_R$, $\widetilde{A}$ and $\widetilde{F}_I$, works as a direct solver; i.e., $v = u$, if and only if

$$\bar{\Pi}_{R,L} \Lambda_L \widetilde{\Pi}_{I,L} = \bar{\Pi}_{R,H} \Lambda_H \widetilde{\Pi}_{I,H} \ . \quad (43)$$

Proof: From (42), the direct solution is obtained if and only if

$$\widetilde{K}\bar{K} = \left[\begin{smallmatrix} 0 & 0 \\ 0 & 0 \end{smallmatrix}\right] \ . \quad (44)$$

Using Theorem 3, the conditions in the diagonal blocks, which guarantee a perfect recovery of the solution, give

$$\begin{aligned} &(I - \widetilde{\Pi}_{I,L} \widetilde{\Delta}^{-1} \widetilde{\Pi}_{R,L} \Lambda_L)(I - \bar{\Pi}_{I,L} \bar{\Delta}^{-1} \bar{\Pi}_{R,L} \Lambda_L) \\ &\quad = \widetilde{\Pi}_{R,H} \widetilde{\Pi}_{R,L} (\bar{\Delta}\widetilde{\Delta})^{-1} \widetilde{\Pi}_{I,L} \bar{\Pi}_{I,H} \Lambda_L \Lambda_H \end{aligned} \quad (45)$$

and

$$\begin{aligned} &(I - \widetilde{\Pi}_{I,H} \widetilde{\Delta}^{-1} \widetilde{\Pi}_{R,H} \Lambda_H)(I - \bar{\Pi}_{I,H} \bar{\Delta}^{-1} \bar{\Pi}_{R,H} \Lambda_H) \\ &\quad = \widetilde{\Pi}_{R,L} \bar{\Pi}_{R,H} (\bar{\Delta}\widetilde{\Delta})^{-1} \widetilde{\Pi}_{I,H} \bar{\Pi}_{I,L} \Lambda_L \Lambda_H \ . \end{aligned} \quad (46)$$

The conditions in the off–diagonal blocks, which take care of aliasing cancellation, give

$$\begin{aligned} &(I - \widetilde{\Pi}_{I,L} \widetilde{\Delta}^{-1} \widetilde{\Pi}_{R,L} \Lambda_L) \bar{\Pi}_{I,L} \bar{\Delta}^{-1} \bar{\Pi}_{R,H} \Lambda_H \\ &\quad = (I - \bar{\Pi}_{I,H} \bar{\Delta}^{-1} \bar{\Pi}_{R,H} \Lambda_H) \widetilde{\Pi}_{I,L} \widetilde{\Delta}^{-1} \widetilde{\Pi}_{R,H} \Lambda_H \end{aligned} \quad (47)$$

and

$$\begin{aligned} &(I - \widetilde{\Pi}_{I,H} \widetilde{\Delta}^{-1} \widetilde{\Pi}_{R,H} \Lambda_H) \bar{\Pi}_{I,H} \bar{\Delta}^{-1} \bar{\Pi}_{R,L} \Lambda_L \\ &\quad = (I - \bar{\Pi}_{I,L} \bar{\Delta}^{-1} \bar{\Pi}_{R,L} \Lambda_L) \widetilde{\Pi}_{I,H} \widetilde{\Delta}^{-1} \widetilde{\Pi}_{R,L} \Lambda_L \ . \end{aligned} \quad (48)$$

Here, all matrices are diagonal and therefore their products commute. None of the eigenvalues of inter–grid filters are zero because they are non–singular. Then, it is safe to multiply by any inverse of these matrices if necessary for simplifications. Since the coarse grid matrices are non–singular, each of the conditions above can be multiplied by $\bar{\Delta}\widetilde{\Delta}$. After this multiplication, using (36) and (37), the simplifications for the four equations independently give the same condition shown in (43). ∎

It is clear from (43) that inter–grid filters satisfying this condition should swap the low– and high–frequency eigenvalues of the system matrix. The mirror of the system matrix fits perfectly for this purpose. The following corollary gives a particular solution which tries to keep the algorithm as simple as possible.

Corollary 2: A red–black harmonic two–grid configuration arranged as shown in Fig. 7a, with non–singular A and such that $\det(\Lambda_L + \Lambda_H) \neq 0$, works as a direct solver with the following configuration:

$$\begin{aligned} \bar{F}_I &= I \ , & \bar{F}_R &= I \ , \\ \widetilde{F}_I &= A^\star \quad \text{and} & \widetilde{F}_R &= I \ . \end{aligned} \quad (49)$$

The coarse grid correction matrices for this configuration are

$$\bar{K} = (\Lambda_L + \Lambda_H)^{-1}\, W \begin{bmatrix} \Lambda_H & -\Lambda_H \\ -\Lambda_L & \Lambda_L \end{bmatrix} V^H \quad \text{and}$$
$$\widetilde{K} = \frac{1}{2}\, W \begin{bmatrix} I & I \\ I & I \end{bmatrix} V^H \,. \tag{50}$$

Proof: Using the eigen–decomposition of filters and Proposition 2 gives

$$\begin{aligned} \bar{\Pi}_I &= I \,, & \bar{\Pi}_R &= I \,, \\ \widetilde{\Pi}_{I,L} &= \Lambda_H \,,\ \widetilde{\Pi}_{I,H} = \Lambda_L \quad \text{and} & \widetilde{\Pi}_R &= I \,. \end{aligned} \tag{51}$$

Using these eigenvalues in (36) and (37) gives $\bar{\Delta} = \Lambda_L + \Lambda_H$ and $\widetilde{\Delta} = 2\Lambda_L\Lambda_H$. Therefore, by Lemma 1 the coarse grid system matrices are invertible. Then, Theorem 4 can be applied and the eigenvalues of inter–grid filters above fulfill the condition (43). Finally, using (51) in Theorem 3 gives (50). ∎

From $\widetilde{K}$ in (50) we see that the nested iteration step is not filtering nor reducing any frequency component of the error. It just equals the gain of all the effects. On the other hand, from $\bar{K}$ in (50) we see that the correction scheme acts as a mirror filter by swapping the low– and high–frequency eigenvalues of the system matrix in the diagonal blocks. The aliasing effect in the off–diagonals is adjusted to cancel the symbols at the same row in $\bar{K}$, so that $\widetilde{K}\bar{K} = 0$.

This solution is particularly simple in the nested iteration step, since only down/up–sampling operations are used. The coarse grid matrix $\bar{A} = \bar{D}A\bar{U}$ has better sparseness than the system matrix A. On the other hand, the sparseness of $\widetilde{A} = \widetilde{D}A^{\star}\widetilde{A}\widetilde{U}$ depends on the structure of down–sampling and non–zeros in A.

When solving Poisson's equation, this solution is equivalent to the total reduction method by Schröder and Trottenberg [7], [8]. The derivation of total reduction methods was based on the structure of a stationary impulse response for LSI systems and thus imposes stronger assumptions on the system.

B. Additive Approach

The second approach is the two–grid algorithm shown in Fig. 7b which uses the structure of the two–channel multi–rate system from Fig. 6. This is a two–grid scheme with two nested iterations working in parallel at red and black coarse grids. The red and black coarse grids work as the two channels of a multi–rate system, but now, linear systems of equations are solved before the interpolation and addition of the two approximations. In a multi–rate system the idea is to reconstruct the input signal (in this case f) but now the idea is to transform this signal into the solution of the linear system.

If this algorithm works as a direct solver then it means that the problem is being factorized into coarse grid sub–problems. The following proposition shows this in terms of a factorization of A^{-1}.

Proposition 4: The system shown in Fig. 7b works as a direct solver; i.e., $v = u$, if and only if the following decomposition applies on the inverse of the system matrix:

$$A^{-1} = \bar{I}_I \bar{A}^{-1} \bar{I}_R + \widetilde{I}_I \widetilde{A}^{-1} \widetilde{I}_R \,. \tag{52}$$

Proof: The approximation error in Fig. 7b is given by $e = u - (\bar{v} + \widetilde{v})$. Using (5) gives

$$e = \left(\bar{K} + \widetilde{K} - I\right) u \tag{53}$$

Then, an exact solution is obtained if and only if $\bar{K} + \widetilde{K} = I$. Using (32) and (33) gives (52). ∎

As opposed to (41), here no cross–terms appear in the decomposition. This reflects the fact that nested iterations run independent of each other. This makes this scheme better suited for parallelization.

This factorization is known in domain decompositions as the *additive Schwartz procedure* [23]. In this procedure the evolution of the approximation error in m iteartions is represented by the *additive operator*, $P_{ad} = K_m + \cdots + K_1 + K_0$, where K_i are coarse grid correction matrices. The classical domain decomposition approach does not work as a direct solver and therefore $P_{ad} \neq I$. Thus, the two–grid configuration in Fig. 7b corresponds to a direct additive Schwartz configuration.

The following theorem establishes conditions on the inter–grid filters to obtain a direct solver.

Theorem 5: A red–black harmonic two–grid configuration arranged as shown in Fig. 7b, with non–singular A, $\bar{A}$, $\bar{F}_R$, $\widetilde{A}$ and $\widetilde{F}_I$, works as a direct solver; i.e., $v = u$, if and only if

$$\bar{\Pi}_{R,L}\widetilde{\Pi}_{R,L}\Lambda_L^2\bar{\Pi}_{I,L}\widetilde{\Pi}_{I,L} = \bar{\Pi}_{R,H}\widetilde{\Pi}_{R,H}\Lambda_H^2\bar{\Pi}_{I,H}\widetilde{\Pi}_{I,H} \,, \tag{54}$$
$$\begin{aligned} &\bar{\Pi}_{R,L}\widetilde{\Pi}_{R,H}\Lambda_L^2\bar{\Pi}_{I,L}\widetilde{\Pi}_{I,L} + \bar{\Pi}_{R,H}\widetilde{\Pi}_{R,H}\Lambda_H^2\bar{\Pi}_{I,H}\widetilde{\Pi}_{I,L} = \\ &\quad \bar{\Pi}_{R,H}\widetilde{\Pi}_{R,L}\Lambda_L^2\bar{\Pi}_{I,L}\widetilde{\Pi}_{I,L} + \bar{\Pi}_{R,H}\widetilde{\Pi}_{R,H}\Lambda_H^2\bar{\Pi}_{I,L}\widetilde{\Pi}_{I,H} \end{aligned} \tag{55}$$

and

$$\begin{aligned} &\bar{\Pi}_{R,L}\widetilde{\Pi}_{R,L}\Lambda_L^2\bar{\Pi}_{I,L}\widetilde{\Pi}_{I,H} + \bar{\Pi}_{R,H}\widetilde{\Pi}_{R,L}\Lambda_H^2\bar{\Pi}_{I,H}\widetilde{\Pi}_{I,H} = \\ &\quad \bar{\Pi}_{R,L}\widetilde{\Pi}_{R,L}\Lambda_L^2\bar{\Pi}_{I,H}\widetilde{\Pi}_{I,L} + \bar{\Pi}_{R,L}\widetilde{\Pi}_{R,H}\Lambda_H^2\bar{\Pi}_{I,H}\widetilde{\Pi}_{I,H} \,. \end{aligned} \tag{56}$$

Proof: From (53) the direct solution is obtained if and only if

$$\bar{K} + \widetilde{K} = \left[\begin{smallmatrix} I & 0 \\ 0 & I \end{smallmatrix}\right] \,. \tag{57}$$

Using Theorem 3, the conditions in the diagonal blocks, which guarantee a perfect recovery of the solution, give

$$\bar{\Pi}_{I,L}\bar{\Delta}^{-1}\bar{\Pi}_{R,L}\Lambda_L + \widetilde{\Pi}_{I,L}\widetilde{\Delta}^{-1}\widetilde{\Pi}_{R,L}\Lambda_L = I \quad \text{and} \tag{58}$$
$$\bar{\Pi}_{I,H}\bar{\Delta}^{-1}\bar{\Pi}_{R,H}\Lambda_H + \widetilde{\Pi}_{I,H}\widetilde{\Delta}^{-1}\widetilde{\Pi}_{R,H}\Lambda_H = I \,. \tag{59}$$

The conditions in the off–diagonal blocks, which take care of aliasing cancellation, give

$$\bar{\Pi}_{I,L}\bar{\Delta}^{-1}\bar{\Pi}_{R,H} - \widetilde{\Pi}_{I,L}\widetilde{\Delta}^{-1}\widetilde{\Pi}_{R,H} = 0 \quad \text{and} \tag{60}$$
$$\bar{\Pi}_{I,H}\bar{\Delta}^{-1}\bar{\Pi}_{R,L} - \widetilde{\Pi}_{I,H}\widetilde{\Delta}^{-1}\widetilde{\Pi}_{R,L} = 0 \,. \tag{61}$$

Here, all matrices are diagonal and therefore their products commute. None of the eigenvalues of inter–grid filters are zero because they are non–singular. Then, it is safe to multiply by any inverse of these matrices if necessary for simplifications. Since the coarse grid matrices are non–singular, each of the conditions above can be multiplied by $\bar{\Delta}\widetilde{\Delta}$. After this multiplication, using (36) and (37), the algebra on the conditions (58) and (59) simplifies to the same condition in (54), and

the algebra on (60) and (61) simplifies to (55) and (56), respectively. ■

These conditions are analogous to Vetterli's conditions (23–25). The analogy is more clear from (58–61) where the only difference with (23–25) is the existence of the matrices $\bar{\Delta}$, $\widetilde{\Delta}$, Λ_L and Λ_H. This indicates the fact that a linear system of equations is being solved.

Again, the mirror of the system matrix can be used to find a solution of these conditions. The following corollary gives a particular solution which tries to keep the algorithm as simple as possible.

Corollary 3: A red–black harmonic two–grid configuration arranged as shown in Fig. 7b, with non–singular A, works as a direct solver with the following configuration:

$$\begin{aligned} \bar{F}_I &= A^\star\,, & \bar{F}_R &= I\,, \\ \widetilde{F}_I &= A^\star \quad \text{and} & \widetilde{F}_R &= I\,. \end{aligned} \tag{62}$$

The coarse grid correction matrices for this configuration are

$$\begin{aligned} \bar{K} &= \frac{1}{2}\,W \begin{bmatrix} I & -I \\ -I & I \end{bmatrix} V^H \quad \text{and} \\ \widetilde{K} &= \frac{1}{2}\,W \begin{bmatrix} I & I \\ I & I \end{bmatrix} V^H\,. \end{aligned} \tag{63}$$

Proof: Using the eigen–decomposition of filters and Proposition 2 gives

$$\begin{aligned} \bar{\Pi}_{I,L} &= \Lambda_H\,, \quad \bar{\Pi}_{I,H} = \Lambda_L\,, & \bar{\Pi}_R &= I\,, \\ \widetilde{\Pi}_{I,L} &= \Lambda_H\,, \quad \widetilde{\Pi}_{I,H} = \Lambda_L \quad \text{and} & \widetilde{\Pi}_R &= I\,. \end{aligned} \tag{64}$$

Using these eigenvalues in (36) and (37) gives $\bar{\Delta} = \widetilde{\Delta} = 2\Lambda_L\Lambda_H$. Therefore, by Lemma 1, the coarse grid system matrices are invertible. Then, Theorem 5 can be applied and the eigenvalues of inter–grid filters fulfill conditions (54–56). Using the eigenvalues from (64) in Theorem 3 gives (63). ■

The coarse grid correction matrices in (63) equal the gain of filtering and aliasing effects. Interestingly, the symbols of $\bar{K}$ and $\widetilde{K}$ correspond to the black and red harmonic aliasing pattern in (16), $\widetilde{N}$ and $\bar{N}$, respectively. The aliasing effect in the off–diagonals have opposed signs between red and black coarse grids, so that $\widetilde{K} + \bar{K} = I$.

Compared with the solution for the multiplicative approach, the additive approach involves more computations. This is because both red and black coarse grid matrices use a mirror filter. On the other hand, this approach is better suited for parallelization. Therefore, both the multiplicative an additive approaches become useful depending on the computational resources available. The multiplicative approach is more convenient in a single processor and the additive approach is more convenient in a multi–core architecture.

VII. Direct Multi–grid Methods

The convergence analysis of previous sections will be valid at each coarse level if harmonic aliasing patterns exist for each coarse system matrix. The following definition introduces the multi–scale property needed on the biorthogonal eigenvectors of the system.

Definition 5 (Multi–grid Harmonic Basis): A *multi–grid harmonic basis* of level 0 is any biorthogonal basis of $\mathbb{C}^n$. A *multi–grid harmonic basis* of level $l > 0$ is a biorthogonal basis of $\mathbb{C}^n$, $n = 2^l n_0$ and $n_0 \in \mathbb{N}^+$, with red–black harmonic aliasing patterns and such that the down–sampled low–frequency eigenvectors form a *multi–grid harmonic basis* of level $l-1$.

The two–grid methods in section VI can be extended to multiple grids if the eigenvectors of a system matrix $A \in \mathbb{C}^{n\times n}$, with $n = 2^l n_0$ and $n_0 = \mathcal{O}(1)$, form a multi–grid harmonic basis of level l.

A. Multiplicative direct multi–grid algorithm

The recursive implementation of the multiplicative approach shown in Fig. 7a is explained in Table I. Here, the difference equation for the number of multiplications performed gives $p(n) = \mathcal{O}(n \log n)$.

Starting from two coarse grids in the first level, the algorithm creates coarser grids which form a partition of the fine grid into more subsets of nodes. In Fig. 8a the sequence of coarse grids visited by the algorithm is shown for $l = 3$. The structure is a W–cycle, well known in multi–grid methods [16]. At each level the partition of nodes is duplicated. For instance, in the coarsest level the grid partition gives

$$\Omega = \Omega_{rrr} + \Omega_{rrb} + \Omega_{rbr} + \Omega_{rbb} + \Omega_{brr} + \Omega_{brb} + \Omega_{bbr} + \Omega_{bbb}\,, \tag{65}$$

where the subindexes from left (fine) to right (coarse) indicate if red or black grids were chosen.

This algorithm has the convenient property that the red coarse system matrix $\bar{A} = \bar{D}A\bar{U}$ reduces the sparseness of the system matrix A. In coarser levels the system matrix might soon become diagonal and the system is solved in linear time. Thus, there are good chances that the structure in Fig. 8a changes from a W–cycle into a V–cycle [16], reducing the computational complexity from $\mathcal{O}(n \log n)$ to $\mathcal{O}(n)$. This is actually what happens when solving Poisson's equation, where this method is equivalent to total reduction methods [7], [8]. In general, this depends on the structure of the system and it will not be study here in depth. The PDE example in section VIII shows a case where the computational complexity is effectively reduced.

B. Additive direct multi–grid algorithm

The recursive implementation of the additive approach shown in Fig. 7b is explained in Table I. Here, the difference equation for the number of multiplications performed gives $p(n) = \mathcal{O}(n \log n)$.

Same as for the multiplicative approach, the algorithm creates coarser grids which form a partition of the fine grid into more subsets of nodes. In Fig. 8b the sequence of coarse grids visited by the algorithm is shown for $l = 3$. The structure is a binary tree that duplicates the number of partitions at each level. The partition at the coarsest level is the same as in (65).

This algorithm is more convenient for parallelization. In fact, as shown in Fig. 7b, a problem separated into red and coarse grids can run in two different processors at the same time. In the coarsest grids of Fig. 8b, a total of eight problems can run in parallel if eight different processors are available.

TABLE I
PSEUDOCODE FOR THE DIRECT MULTI–GRID ALGORITHM FOLLOWING MULTIPLICATIVE AND ADDITIVE APPROACHES TO SOLVE $Au = f$. THE MATRIX $A^\star$ REPRESENTS THE MIRROR OF A ACCORDING TO DEFINITION 3.

Task	Products
$u = \texttt{DMG\_multiplicative}(A, f, n)$	$p(n)$
`if` $n > n_0$, $n_0 = \mathcal{O}(1)$	
$\bar{f} = \bar{D} f$	0
$\bar{A} = \bar{D} A \bar{U}$	0
$\bar{v} = \texttt{DMG\_multiplicative}(\bar{A}, \bar{f}, \frac{n}{2})$	$p(\frac{n}{2})$
$v_0 = \bar{U} \bar{v}$	0
$r = f - A v_0$	$\mathcal{O}(n)$
$\widetilde{r} = \widetilde{D} r$	0
$\widetilde{I}_I = A^\star \widetilde{U}$	0
$\widetilde{A} = \widetilde{D} A \widetilde{I}_I$	$\mathcal{O}(n)$
$\widetilde{e} = \texttt{DMG\_multiplicative}(\widetilde{A}, \widetilde{r}, \frac{n}{2})$	$p(\frac{n}{2})$
$e_0 = \widetilde{I}_I \widetilde{e}$	$\mathcal{O}(n)$
$u = v_0 + e_0$	0
`return`(u)	
`else`	
`return`$(A^{-1} f)$	$\mathcal{O}(1)$

Task	Products
$u = \texttt{DMG\_additive}(A, f, n)$	$p(n)$
`if` $n > n_0$, $n_0 = \mathcal{O}(1)$	
$\bar{f} = \bar{D} f$	0
$\bar{I}_I = A^\star \bar{U}$	0
$\bar{A} = \bar{D} A \bar{I}_I$	$\mathcal{O}(n)$
$\bar{v} = \texttt{DMG\_additive}(\bar{A}, \bar{f}, \frac{n}{2})$	$p(\frac{n}{2})$
$\widetilde{f} = \widetilde{D} f$	0
$\widetilde{I}_I = A^\star \widetilde{U}$	0
$\widetilde{A} = \widetilde{D} A \widetilde{I}_I$	$\mathcal{O}(n)$
$\widetilde{v} = \texttt{DMG\_additive}(\widetilde{A}, \widetilde{f}, \frac{n}{2})$	$p(\frac{n}{2})$
$u = \bar{I}_I \bar{v} + \widetilde{I}_I \widetilde{v}$	$\mathcal{O}(n)$
`return`(u)	
`else`	
`return`$(A^{-1} f)$	$\mathcal{O}(1)$

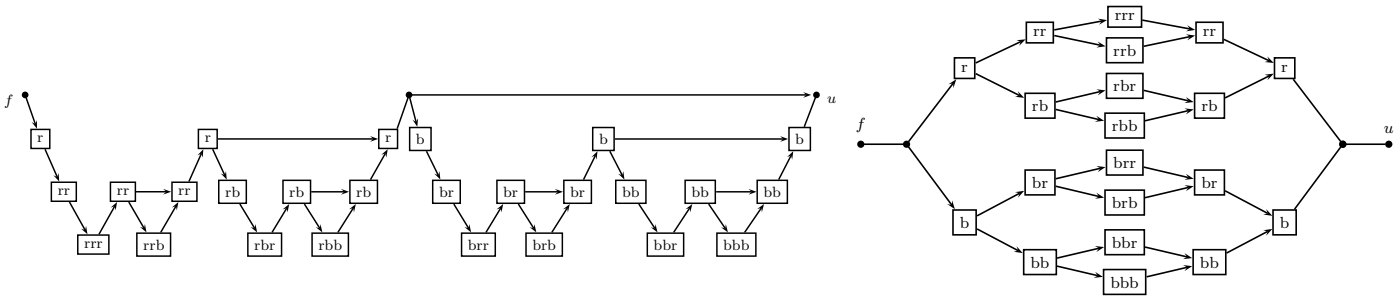

(a) Multiplicative algorithm (b) Additive algorithm

Fig. 8. Dataflow diagram showing the sequence of coarse grids visited when using multiplicative or additive approaches. The sequence of letters in each box indicates the coarse grid where computations take place. Inside of the boxes, from left to right, letters 'r' or 'b' indicates red or black grids, respectively, selected from fine to coarse levels. The execution time moves from left to right. The source vector f enters from the left end and the exact solution u is obtained at the right end. Boxes in the same horizontal position indicate grids where computations can run in parallel. In the multiplicative approach, coarse grids are visited sequentially through a W–cycle, not allowing parallel computations. In the additive approach, coarse grids are visited through a binary tree, allowing parallel computations.

Thus, under the assumption of a multi–grid harmonic basis of level l, with $n = 2^l n_0$ and $n_0 = \mathcal{O}(1)$, if $\mathcal{O}(n)$ processors are available then the computational complexity reduces from $\mathcal{O}(n \log n)$ to $\mathcal{O}(\log n)$. Unfortunately, such an ideal situation rarely exists. A similar scenario happens in a *sensor network* where a set of sensors are deployed over an area where they measure the source vector of a linear model. Each sensor performs computations in–site and can be associated with a small group of grid nodes. In this case, communications between sensors prevent the algorithm to reach the ideal time complexity to solve the model equations. Nevertheless, this approach provides a simple way to parallelize the solution of a linear system using all the available computational resources.

VIII. EXAMPLES

Two examples are considered: deblurring an image and solving a PDE. Both problems solve the linear system (1) for a two–dimensional operator A with stationary impulse response

$$\frac{1}{256}\begin{bmatrix} 4 & 6 & 12 & 6 & 4 \\ 6 & 9 & 18 & 9 & 6 \\ 12 & 18 & \underline{36} & 18 & 12 \\ 6 & 9 & 18 & 9 & 6 \\ 4 & 6 & 12 & 6 & 4 \end{bmatrix} \quad \text{and} \quad \begin{bmatrix} & -1 & \\ -1 & \frac{\left(4-(\frac{\pi}{12})^2\right)}{-1} & -1 \\ & -1 & \end{bmatrix} \tag{66}$$

for the blurring and the differential operator, respectively. The underlines in (66) denote the diagonal elements. In both problems the size of the discrete domain is set to $n = 128 \times 128$ and periodic boundary conditions are considered.

In the deblurring problem, an unkown image u passes through an imperfect optical system that spreads each pixel value over its neighbouring pixels and gives the observed blurred image f. This blurring effect needs to be removed by solving the linear system. This is not a straightforward problem to be solved by multi–grid techniques since the system is represented by an integral matrix (low–pass filter) instead of a differential matrix (high–pass filter). On one hand, multi–grid iterative methods have been adapted to solve this problem, see for example [37], [38]. And on the other hand, the direct

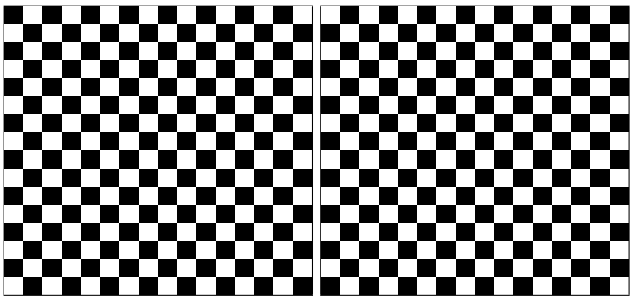

(a) $\Omega = \Omega_r + \Omega_b$

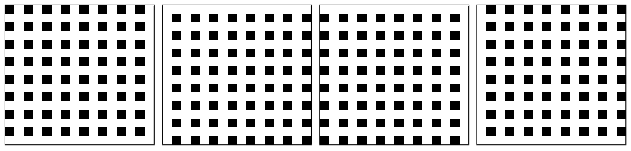

(b) $\Omega = \Omega_{rr} + \Omega_{rb} + \Omega_{br} + \Omega_{bb}$

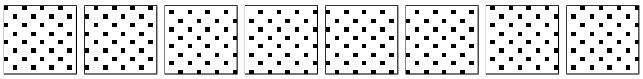

(c) $\Omega = \Omega_{rrr} + \Omega_{rrb} + \Omega_{rbr} + \Omega_{rbb} + \Omega_{brr} + \Omega_{brb} + \Omega_{bbr} + \Omega_{bbb}$

Fig. 9. Red–black partitions of nodes for a 2D square domain Ω of size $n = 16 \times 16$. Dark squares indicate the selected nodes. The same pattern is used in the examples of Section VIII on a domain of size $n = 128 \times 128$.

multi–grid solvers work naturally regardless of the operator being integral or differential.

In the PDE problem, the operator represents the finite–difference discretization of Helmholtz's equation $-\nabla^2 u - k^2 u = f$ on a square domain with unit step size and wavenumber $k = \frac{\pi}{12}$. The equation needs to be solved for a known source vector f. A sparse source vector will be considered, which represents a common situation in PDEs where non–zero values of sources are normally located at boundaries or point sources.

Both systems are invariant under space shifts and therefore the eigenvectors are given by harmonic functions $(W)_{i,j} = \exp\left(\sqrt{-1}\,\frac{2\pi}{n} ij\right)$. After proper reordering, the basis has harmonic aliasing patterns if the down–sampling pattern shown in Fig. 9 is used. A checkerboard down–sampling as shown in Fig. 9a gives a mirror matrix $A^\star$ with stationary impulse response

$$\frac{1}{256}\begin{bmatrix} 4 & -6 & 12 & -6 & 4 \\ -6 & 9 & -18 & 9 & -6 \\ 12 & -18 & \underline{36} & -18 & 12 \\ -6 & 9 & -18 & 9 & -6 \\ 4 & -6 & 12 & -6 & 4 \end{bmatrix} \quad \text{and} \quad \begin{bmatrix} 1 \\ 1 \;\; \frac{4-(\frac{\pi}{12})^2}{1} \;\; 1 \end{bmatrix} \qquad (67)$$

for the blurring and the differential operator, respectively.

An important problem arises naturally for systems in two or more dimensions. The down/up–sampling by a factor of 2 is not enough to reduce the impulse response of the product $AA^\star$. Then, the impulse response of system matrices grows larger and larger in coarse grids. An example for the impulse response of a Laplacian operator is shown in Fig. 10. The same problem appears in other direct multi–grid solvers like total and partial (or cyclic) reduction methods [7]–[9].

In Fig. 11a and 11b a blurred image (known) and a deblurred image (unkown) are shown. In Fig. 12a and 12b the intermediate solutions of a two–grid multiplicative approach are shown. In this case the red coarse system matrix represents a smaller blurring mask. Therefore, the nested iteration step removes some of the blurring effects and obtains a good initial approximation. The black coarse system adds the correction with all the missing details. In Fig. 13a, 13c and 13e the intermediate solutions of an additive multi–grid approach are shown for three coarse levels. Here, the solutions from each coarse grid gives the same amount of detail to construct the deblurred image.

In Fig. 11c and 11d a solution of Helmholtz's equation is shown for a sparse source vector. In Fig. 12c and 12d the intermediate solutions of a two–grid multiplicative approach are shown. Here, the red coarse system matrix is diagonal and the source vector is sparse. Therefore, the initial approximation of nested iteration is sparse. Then, the correction scheme adds the remaining component which, in this case, is the most significant part of the solution. In Fig. 13b, 13d and 13f the solutions at coarse grids are shown by using an additive approach. Each of the 4 point sources in f appears in one of the coarse grids Ω_{rr}, Ω_{rb}, Ω_{br} and Ω_{bb}. At the third coarse level the point sources only appear in Ω_{rrr}, Ω_{rbr}, Ω_{brb} and Ω_{bbb}. Therefore, each point source appears only once at each coarse level. This is a consequence of the down–sampling restriction and makes this approach an effective way to obtain the Green's function of a system for specific point sources.

IX. Comparisons

In terms of computational complexity, under general assumptions the direct multi–grid algorithms do not compete against iterative solvers. For instance, the full multi–grid algorithm is an iterative solver that can be efficiently configured for LSI systems and reaches computational complexity $\mathcal{O}(n)$, whereas the direct multi–grid approaches need $\mathcal{O}(n \log n)$ computations. In specific cases, including the solution of Poisson's equation, the multiplicative approach reduces the W–cycle in Fig. 8a to a V–cycle where $\mathcal{O}(n)$ computations are needed. Still, this was already known for these cases where the multiplicative approach is equivalent to the total reduction method [7], [8].

On the other hand, the direct multi–grid methods are competitive compared with other direct solvers. In terms of computational complexity, for LSI systems the direct–multi–grid solvers stand along with FFT–based solvers, needing $\mathcal{O}(n \log n)$ computations [15]. The comparison with sparse LU solvers is not clear in general since the performance of these solvers strongly depends on the fill–in during the factorization process [5]. In terms of memory space it is important not to store all the coarse grid matrices at once as this soon becomes prohibitive, scaling as $\mathcal{O}(n \log n)$. The number of variables needed to run a direct multi–grid solver is between $2n$ and $3n$ depending on the implementation, although the grow of impulse responses shown in Fig. 10 might increase this number depending on the problem.

Since direct multi–grid solvers make internal use of a direct solver in the coarsest grids, these methods can also be used to boost a different direct solver. For example, if an efficient direct solver only uses a single processor then the additive approach can be used to parallelize this solver.

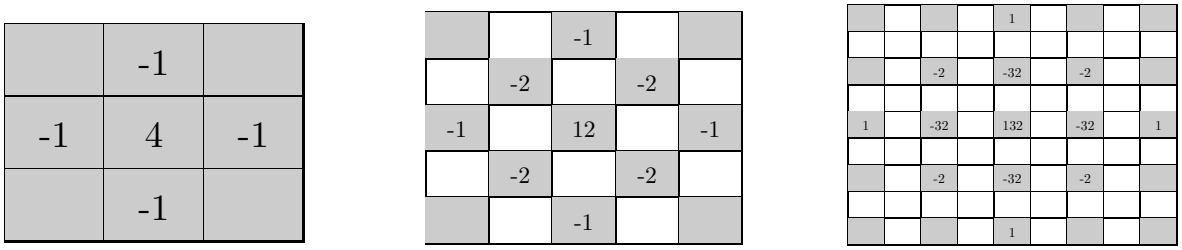

(a) Impulse response in Ω (b) Impulse response in Ω_r (c) Impulse response in Ω_{rr}

Fig. 10. Impulse response coefficients from a finite–difference discretization of the Laplacian operator: $-\nabla^2$. The coarse grid system matrices obtained with mirror filters give impulse responses that grow in coarse grids.

(a) Source vector: f. (b) Exact solution: u. (c) Source vector: f. (d) Exact solution: u.

Fig. 11. In the first example, the convolution of an image and the mask $\frac{1}{256}$ $[2\ 3\ 6\ 3\ 2]^T[2\ 3\ 6\ 3\ 2]$ forms the source vector in 11a. The exact solution is shown in 11b. In the second example, Helmholtz's equation, $-\nabla^2 u - k^2 u = 0$ with $k = \frac{\pi}{12}$, is solved in a square domain with periodic boundary conditions. In 11c the source vector is equal to 1 in four neighboring nodes at the center of the figure and zero elsewhere. The exact solution is shown in 11d.

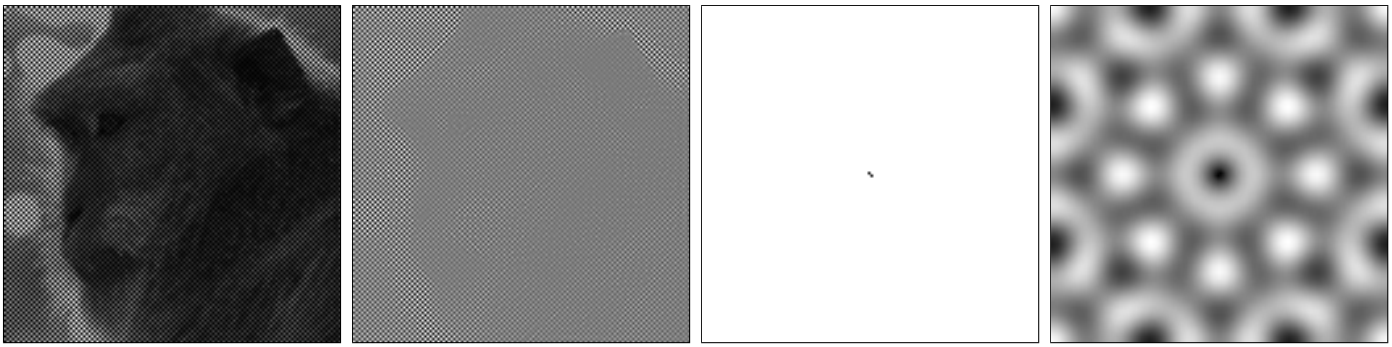

(a) v_0 for f in Fig. 11a (b) e_0 for f in Fig. 11a (c) v_0 for f in Fig. 11c (d) e_0 for f in Fig. 11c

Fig. 12. Intermediate solutions of the direct two–grid multiplicative approach from Fig. 7a. In 12a and 12b the intermediate solutions are shown for a deblurring problem. In 12c and 12d the intermediate solutions are shown for a PDE problem.

X. Conclusions

Numerical methods to solve linear systems of equations were obtained based on the similarities of the full two–grid algorithm and perfect reconstruction filter banks. The two alternatives, multiplicative and additive, correspond to direct Schwartz domain decomposition methods based on a partition of the original domain. The additive approach can be used to parallelize the problem among all the available processors, whereas the multiplicative approach is more efficient in a single processor.

Future research will focus on the application of these algorithms in systems that are not LSI. On one hand, the algorithms are ready to work on systems that are known to have harmonic aliasing patterns but more numerical studies are necessary. And, on the other hand, the most challenging problem is to understand the physical and geometrical implications of harmonic aliasing patterns. This is essential to construct practical methods to check aliasing patterns and be able to use these methods in more challenging problems.

Appendix A
Proof of Theorem 1

Proof: The proof of the red harmonic aliasing pattern being equivalent to (18) is due to Navarrete and Coyle [11]. The proof of the black harmonic aliasing pattern being equivalent to (19) follows the same reasoning. Given the partition

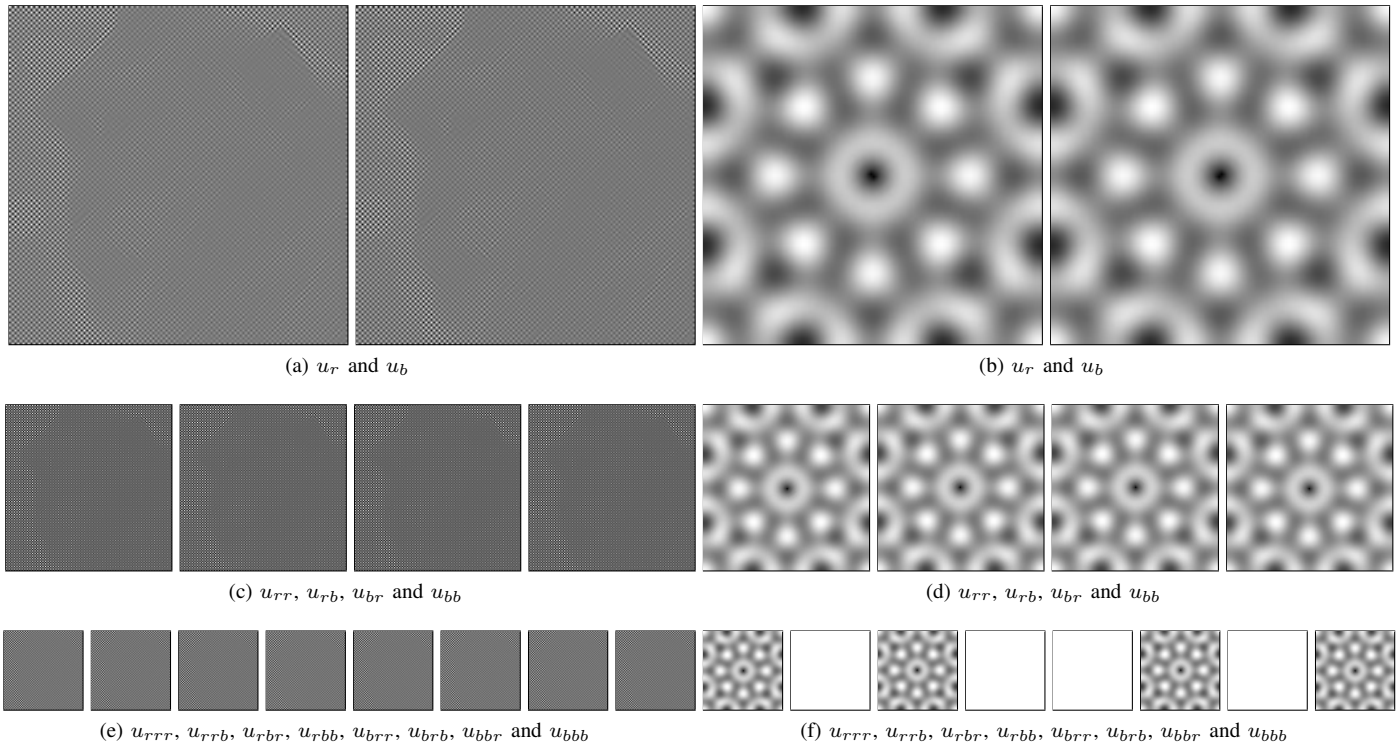

(a) u_r and u_b (b) u_r and u_b

(c) u_{rr}, u_{rb}, u_{br} and u_{bb} (d) u_{rr}, u_{rb}, u_{br} and u_{bb}

(e) u_{rrr}, u_{rrb}, u_{rbr}, u_{rbb}, u_{brr}, u_{brb}, u_{bbr} and u_{bbb} (f) u_{rrr}, u_{rrb}, u_{rbr}, u_{rbb}, u_{brr}, u_{brb}, u_{bbr} and u_{bbb}

Fig. 13. Intermediate solutions of the direct multi–grid additive approach from Fig. 7b. Considering the sources in Fig. 11a and 11c for the deblurring and PDE problems, respectively, the exact solution is given by: $u = u_r + u_b$ at the first coarse level in Fig. 13a and 13b, respectively; $u = u_{rr} + u_{rb} + u_{br} + u_{bb}$ at the second coarse level in Fig. 13c and 13d, respectively; and $u = u_{rrr} + u_{rrb} + u_{rbr} + u_{rbb} + u_{brr} + u_{brb} + u_{bbr} + u_{bbb}$ at the third coarse level in Fig. 13e and 13f, respectively.

of eigenvectors $W = [W_L W_H]$ and $V = [V_L V_H]$, the black harmonic aliasing pattern can be written as the following set of biorthogonal relationships

$$(\widetilde{D}V_L)^H(\widetilde{D}W_L) = \tfrac{1}{2}\, I\,, \tag{68}$$

$$(\widetilde{D}V_L)^H(\widetilde{D}W_H) = -\tfrac{1}{2}\, I\,, \tag{69}$$

$$(\widetilde{D}V_H)^H(\widetilde{D}W_L) = -\tfrac{1}{2}\, I \quad \text{and} \tag{70}$$

$$(\widetilde{D}V_H)^H(\widetilde{D}W_H) = \tfrac{1}{2}\, I\,. \tag{71}$$

Since W and V form a biorthogonal basis,

$$\begin{aligned} WV^H &= W_L V_L^H + W_H V_H^H \\ &= I\,. \end{aligned}$$

Pre-multiplying by $\widetilde{D}$ and post-multiplying by $\widetilde{U}$ gives

$$\begin{aligned} (\widetilde{D}W)(\widetilde{D}V)^H &= (\widetilde{D}W_L)(\widetilde{D}V_L)^H + (\widetilde{D}W_H)(\widetilde{D}V_H)^H \\ &= I\,. \end{aligned} \tag{72}$$

First, (19) is assumed. Then, equation (72) immediately implies the set of biorthogonal relationships above, and the black harmonic aliasing pattern is fulfilled. Second, the black harmonic aliasing pattern is assumed. Pre–multiplying (72) by $(\widetilde{D}V_L)^H$ and using equations (68) and (69) gives $\widetilde{D}V_L = -\widetilde{D}V_H$. Similarly, post–multiplying (72) by $\widetilde{D}W_H$ and using equations (69) and (71) gives $\widetilde{D}W_L = -\widetilde{D}W_H$. Therefore, the black harmonic aliasing pattern implies (19). ■

Appendix B
Proof of Lemma 1

Proof: The proof of (34) is due to Navarrete and Coyle [11]. The proof of (35) follows from

$$\widetilde{A}^{-1} = \left\{\widetilde{D}\widetilde{F}_R A \widetilde{F}_I \widetilde{U}\right\}^{-1} \tag{73}$$

$$= \left\{(\widetilde{D}W)\widetilde{\Pi}_R \Lambda \widetilde{\Pi}_I (\widetilde{D}V)^H\right\}^{-1} \tag{74}$$

$$= \left\{(\widetilde{D}W_L)\widetilde{\Delta}(\widetilde{D}V_L)^H\right\}^{-1} \tag{75}$$

$$= 4\,(\widetilde{D}W_L)\widetilde{\Delta}^{-1}(\widetilde{D}V_L)^H\,, \tag{76}$$

where (30) is used in (73), the eigen–decompositions of filters is used in (74), Theorem 1 is used in (75) and the biorthogonal relationships (68) to (71) are used in (76). ■

Appendix C
Proof of Theorem 3

Proof: The proof of (38) is due to Navarrete and Coyle [11]. The proof of (39) follows from

$$\widetilde{K} = I - \widetilde{F}_I \widetilde{U} \widetilde{A}^{-1} \widetilde{D} \widetilde{F}_R A \tag{77}$$

$$= I - 4\, W \widetilde{\Pi}_I (V^H \widetilde{U} \widetilde{D} W_L) \widetilde{\Delta}^{-1} (V_L^H \widetilde{U} \widetilde{D} W) \widetilde{\Pi}_R \Lambda V^H \tag{78}$$

$$= WV^H - 4\, W \widetilde{\Pi}_I \left(\tfrac{1}{2}\begin{bmatrix} I \\ -I \end{bmatrix}\right) \widetilde{\Delta}^{-1} \left(\tfrac{1}{2}\begin{bmatrix} I & -I \end{bmatrix}\right) \widetilde{\Pi}_R \Lambda V^H \tag{79}$$

$$= W \begin{bmatrix} I - \widetilde{\Pi}_{I,L}\widetilde{\Delta}^{-1}\widetilde{\Pi}_{R,L}\Lambda_L & \widetilde{\Pi}_{I,L}\widetilde{\Delta}^{-1}\widetilde{\Pi}_{R,H}\Lambda_H \\ \widetilde{\Pi}_{I,H}\widetilde{\Delta}^{-1}\widetilde{\Pi}_{R,L}\Lambda_L & I - \widetilde{\Pi}_{I,H}\widetilde{\Delta}^{-1}\widetilde{\Pi}_{R,H}\Lambda_H \end{bmatrix} V^H\,. \tag{80}$$

where (30) is used in (77), the eigen–decomposition of filters and Lemma 1 are used in (78), definition 2 is used in (79) and the partition of eigenvalues is used in (80). ■

ACKNOWLEDGMENT

The author would like to thank Edward J. Coyle, Cornelis W. Oosterlee, James G. Nagy, Patricio Parada and Jorge Silva, as well as the associate editor and reviewers for their comments and references that significantly improved the quality of this publication.

REFERENCES

[1] Y. Saad, *Iterative Methods for Sparse Linear Systems*. Boston: PWS, 1996.
[2] W. Hackbusch, *Iterative Solution of Large Sparse Systems of Equations*, ser. Applied Mathematical Sciences. New York, NY, USA: Springer, 1993.
[3] J. R. Norris, *Markov Chains*, ser. Cambridge Series in Statistical and Probabilistic Mathematics. Cambridge, UK: Cambridge University Press, 1998.
[4] J. E. Dennis and R. B. Schnabel, *Numerical Methods for Unconstrained Optimization and Nonlinear Equations*. Prentice–Hall, 1983.
[5] I. S. Duff, A. M. Erisman, and J. K. Reid, *Direct Methods for Sparse Matrices*. Oxford: Clarendon Press, 1986.
[6] J. J. Dongarra, I. S. Duff, D. C. Sorensen, and H. A. van der Vorst, *Numerical Linear Algebra for High Performance Computers*. Philadelphia, PA, USA: Society for Industrial and Applied Mathematics, 1998.
[7] J. Schröder and U. Trottenberg, "Reduktionsverfahren für differenzengleichungen bei randwertaufgaben I," *Numerische Mathematik*, vol. 22, pp. 37–68, June 1973.
[8] J. Schröder, U. Trottenberg, and H. Reutersberg, "Reduktionsverfahren für differenzengleichungen bei randwertaufgaben II," *Numerische Mathematik*, vol. 26, pp. 429–459, January 1976.
[9] B. L. Buzbee, G. H. Golub, and C. W. Nielson, "On direct methods for solving Poisson's equations," *SIAM Journal on Numerical Analysis*, vol. 7, pp. 627–656, 1970.
[10] D. Ginesa, G. Beylkin, and J. Dunnc, "LU factorization of non–standard forms and direct multiresolution solvers," *Applied and Computational Harmonic Analysis*, vol. 5, no. 2, pp. 156–201, April 1998.
[11] P. Navarrete and E. J. Coyle, "A semi–algebraic approach that enables the design of inter–grid operators to optimize multigrid convergence," *Numerical Linear Algebra with Applications*, vol. 15, no. 2–3, pp. 219–247, March 2008.
[12] ——, "Mobility models based on correlated random walks," in *Proceedings of the 5th International Conference on Mobile Technology, Applications, and Systems, Mobility Conference 2008*, ser. Mobility Conference, J. Lin, H. Chao, and P. Chong, Eds. Yilan, Taiwan: ACM, September 2008, pp. 1–8.
[13] A. Brandt, "Rigorous quantitative analysis of multigrid, I: Constant coefficients two-level cycle with l2-norm," *SIAM J. Numer. Anal.*, vol. 31, no. 6, pp. 1695–1730, 1994.
[14] ——, "Multi–level adaptive solutions to boundary–value problems," *Math. Comp.*, vol. 31, pp. 333–390, 1977.
[15] U. Trottenberg, C. W. Oosterlee, and A. Schüller, *Multigrid*. London: Academic Press, 2000.
[16] W. L. Briggs, V. E. Henson, and S. F. McCormick, *A Multigrid Tutorial*, 2nd ed. SIAM, 2000.
[17] P. P. Vaidyanathan, *Multirate Systems And Filter Banks*. Englewood Cliffs: Prentice Hall, 1993.
[18] S. Dahlke and A. Kunoth, "Biorthogonal wavelets and multigrid," in *Adaptive Methods – Algorithms, Theory and Applications*, ser. Notes on Numerical Fluid Mechanics, vol. 46. Braunschweig: Vieweg, 1994, pp. 99–119.
[19] D. De Leon, "Wavelet techniques applied to multigrid methods," Department of Mathematics UCLA, UCLA Mathematics Department CAM Report 00-42, December 2000.
[20] G. Wang, R. W. Dutton, and J. Hou, "A fast wavelet multigrid algorithm for solution of electromagnetic integral equations," *Microwave and Optical Technology Letters*, vol. 24, no. 2, pp. 86–91, 2000.
[21] F. H. Pereira, S. L. L. Verardi, and S. I. Nabeta, "A wavelet-based algebraic multigrid preconditioner for sparse linear systems," *Applied Mathematics and Computation*, vol. 182, no. 2, pp. 1098–1107, 2006.
[22] V. M. García, L. Acevedo, and A. M. Vidal, "Variants of algebraic wavelet-based multigrid methods: Application to shifted linear systems," *Applied Mathematics and Computation*, vol. 202, no. 1, pp. 287–299, 2008.
[23] A. Toselli and O. Widlund, *Domain Decomposition Methods – Algorithms and Theory*, ser. Springer Series in Computational Mathematics. Springer, 2004, vol. 34.
[24] P. Frederickson and O. McBryan, "Parallel superconvergent multigrid," in *Multigrid Methods: Theory, Applications, and Supercomputing*, S. F. McCormick, Ed. Marcel Dekker, New York, 1988, pp. 195–210.
[25] W. Hackbusch, "A new approach to robust multi–grid solvers," in *ICIAM'87: Proceedings of the First International Conference on Industrial and Applied Mathematics*. Philadelphia: Society for Industrial and Applied Mathematics, 1988, pp. 114–126.
[26] ——, "The frequency decomposition multigrid method, part I: Application to anisotropic equations," *Numer. Math.*, vol. 56, pp. 229–245, 1989.
[27] T. F. Chan and R. S. Tuminaro, "Analysis of a parallel multigrid algorithm," in *Proceedings of the Fourth Copper Mountain Conference on Multigrid Methods*, J. Mandel, S. F. McCormick, J. E. Dendy, C. Farhat, G. Lonsdale, S. V. Parter, J. W. Ruge, and K. Stüben, Eds. Philadelphia: SIAM, 1989, pp. 66–86.
[28] P. Wesseling, *An Introduction to Multigrid Methods*. Chichester: John Wiley and Sons, 1992.
[29] M. Vetterli and J. Kovačević, *Wavelets and Subband Coding*. Englewood Cliffs: Prentice Hall, 1995.
[30] M. Vetterli, "Filter banks allowing perfect reconstruction," *Signal Processing*, vol. 10, no. 3, pp. 219–244, April 1986.
[31] P. P. Vaidyanathan, "Quadrature mirror filter banks, M–band extensions and perfect–reconstruction techniques," *IEEE ASSP Mag.*, vol. 4, no. 3, pp. 4–20, July 1987.
[32] A. Croisier, D. Esteban, and C. Galand, "Perfect channel splitting by use of interpolation/decimation/tree decomposition techniques," in *Proceedings of the Int. Conf. on Inform. Sciences Systems*, Patras, Greece, August 1976, pp. 443–446.
[33] F. Mintzer, "Filters for distortion–free two–band multirate filter banks," *IEEE Trans. Acoust., Speech, Signal Process.*, vol. 33, no. 3, pp. 626–630, June 1985.
[34] M. J. Smith and T. P. Barnwell III, "A procedure for designing exact reconstruction filter banks," in *Proc. IEEE Int. Conf. Acoust., Speech, Signal Process.*, San Diego, CA, March 1984.
[35] S. Mallat, *A Wavelet Tour of Signal Processing*. Academic Press, 1998.
[36] G. Strang and T. Nguyen, *Wavelets and Filter Banks*. Wellesley–Cambridge Press, 1996.
[37] M. Donatelli, "A multigrid for image deblurring with Tikhonov regularization," *Numerical linear algebra with applications*, vol. 12, no. 8, pp. 715–729, October 2005.
[38] Q. Chang, J. Xu, and W. Wang, "A method for total variation-based reconstruction of noisy and blurred images," in *Image Processing Based on Partial Differential Equations*, X.-C. Tai, K.-A. Lie, T. F. Chan, and O. S., Eds. Springer, 2007, pp. 95–108.

Pablo Navarrete Michelini was born in Santiago, Chile. He received the B.Sc. in Physics (2001), B.Sc. in Electrical Engineering (2001) and the Electrical Engineer Degree (2002), from Universidad de Chile at Santiago. He received the Ph.D. degree in Electrical Engineering from Purdue University at West Lafayette, in 2008.

He worked as a research intern in CIMNE at Technical University of Catalonia in 2006, and as a visitor student research collaborator at Princeton University at Princeton, NJ, in 2006–2007. He is Assistant Professor in the Department of Electrical Engineering at Universidad de Chile. His major interests are the application of signal processing tools in problems of scientific computing and especially those based on multi–level techniques.